ADVANCED FUNCTIONAL MATERIALS
www.afm-journal.de

Review on 3D Printing of Bioinspired Structures for Surface/Interface Applications

Qingqing He, Tengteng Tang, Yushun Zeng, Nadine Iradukunda, Brandon Bethers, Xiangjia Li, and Yang Yang**

Natural organisms have evolved a series of versatile functional biomaterials and structures to cope with survival crises in their living environment, exhibiting outstanding properties such as superhydrophobicity, anisotropy, and mechanical reinforcement, which have provided abundant inspiration for the design and fabrication of next-generation multi-functional devices. However, the lack of available materials and limitations of traditional manufacturing methods for complex multiscale structures have hindered the progress in bio-inspired manufacturing of functional structures. As a revolutionary emerging manufacturing technology, additive manufacturing (i.e., 3D printing) offers high design flexibility and manufacturing freedom, providing the potential for the fabrication of intricate, multiscale, hierarchical, and multi-material structures. Herein, a comprehensive review of current 3D printing of surface/interface structures, covering the applied materials, designs, and functional applications is provided. Several bio-inspired surface structures that have been created using 3D printing technology are highlighted and categorized based on their specific properties and applications, some properties can be applied to multiple applications. The optimized designs of these 3D-printed bio-inspired surfaces offer a promising prospect of low-cost, high efficiency, and excellent performance. Finally, challenges and opportunities in field of fabricating functional surface/interface with more versatile functional material, refined structural design, and better cost-effective are discussed.

1. Introduction

Biological architectures inspire the design of next-generation interfacial surfaces through specially evolved hierarchical structures with dimensions spanning from the nanoscale to macroscale.[1–8] Several living organisms evolved complex structures that exhibit unique interfacial functions such as superhydrophobicity,[9] drag force reduction,[10] anisotropic liquid transportation,[11] fog harvesting,[12] and painless insertion.[13] For example, the multiscale structures of the legs of water striders exhibit outstanding superhydrophobicity, enabling floating on the water surface.[14] Various plants and animals such as lotus, rice, poplar, rose, butterfly, and cicada, demonstrated structures revealing self-cleaning properties due to excellent superhydrophobicity.[15] Besides the special wettability performance, other interfacial properties are critical to evolve for survival.[10,16] For example, the shark skin possesses microstructures, which exhibit remarkable drag force reduction underwater so that it can swim faster than its prey.[10] Another good example is the leaves of water fern *Salvinia Molesta*, which demonstrate superior long-term air-retention capability, especially in a turbulent flow environment, due to the evolved hierarchical architectures.[16] The uniqueness of such structures is the combination of features with different wettability including wrinkled hydrophilic patches on superhydrophobic eggbeater hairs.[16] The hydrophilic patches pin the air-water interface to the tips of the eggbeater hairs and prevent the formation and detachment of air bubbles, which stabilizes air layers even in turbulent conditions and low-pressure scenarios ('*Salvinia Effect*') .[16] The trapped air layer can help the leaves float on the surface of the water and dramatically reduce the drag force.[16]

Moreover, multiscale biological structures and material systems in plants comprise the unique capability of anisotropic water transportation because of controllable wettability.[11] For example, the peristome of *Nepenthes alata* shows an essential trapping mechanism that benefits from special surface topography, leading to anisotropic friction and liquid transportation.[11] In addition, biological multiscale structures, and

Q. He, B. Bethers, Y. Yang
Department of Mechanical Engineering
San Diego State University
San Diego, CA 92182, USA
E-mail: yyang10@sdsu.edu
T. Tang, N. Iradukunda, X. Li
Department of Aerospace and Mechanical Engineering
School for Engineering of Matter
Transport and Energy
Arizona State University
Tempe, AZ 85287, USA
E-mail: xiangjia.li@asu.edu
Y. Zeng
Alfred E. Mann Department of Biomedical Engineering
Viterbi School of Engineering
University of Southern California
Los Angeles, CA 90089, USA

The ORCID identification number(s) for the author(s) of this article can be found under https://doi.org/10.1002/adfm.202309323

DOI: 10.1002/adfm.202309323

Table 1. Advantages and disadvantages of varies 3D printing techniques.

Additive manufacturing techniques	Advantages	Disadvantages
Fused Deposition Modeling (FDM)	– Affordable and accessible	– Objects with visible layer lines
	– Wide range of thermoplastic materials	– Limited Material Properties
	– Large build volumes	– Require post-processing
Stereolithography (SLA)	– High level of precision	– Resin handling can be messy
	– Wide Material Compatibility	– Smaller build volumes
	– Fast Printing	– More expensive than FDM
Selective Laser Sintering (SLS)	– Producing complex and intricate structures	– Materials can be expensive
	– Strong and durable	– SLS machines are more complex
Selective Laser Melting (SLM)	– Minimal Post-Processing	– SLS powder requires careful management
Inkjet Printing	– High levels of detail and resolution	– Slow printing speed
	– Full-color printing	– Materials can be more expensive
	– Does not require support structures	– Achieving strong layer-to-layer adhesion in inkjet 3D printing can be challenging
Digital Light Processing (DLP)	– High resolution and high speed	– Limited material compatibility
	– Large build volume	– Post-processing requirements
Binder Jetting	– Material variety	– Lower resolution
	– Affordability	– Require support structures
Two-Photon Polymerization (TPP)	– Complex geometries	– Limited build volume
	– Non-layered printing	– High equipment cost
Laser Engineered Net Shaping (LENS)	– High density and strength	– Result in heat-affected zone
	– Repair and refurbishment	– Rough surface finish

multifunctional material systems yield fog-harvesting capability in living organisms.[12,17–19] For instance, cactus can live in harsh environments because its multiscale spines with grooves and barbs can collect water from dry air. While desert beetles are wonderfully adapted to desert life as the hybrid wettability of bumps allows water to condense more freely.[12,19] After the water is collected, the gathered water will be directionally transported by the hydrophobic structures.[19] Animal structures and material systems present distinct protective performances in terms of rigidity.[13,20–22] For instance, a mosquito can insert a needle-like probe into the skin without pain due to the combination of soft and hard parts on the proboscis.[13] Overall, nature provides us with many biological interfacial structures and smart materials systems that inspired lots of innovations in diverse fields.[23] Performance modification using biological structures and material systems is desired and sometimes is critical to achieve certain interfacial functionality.[24] It raises a question to scientists about how to reproduce such complex biological structures and material systems that are optimized for real applications.

Several interfacial surfaces were fabricated based on the aforementioned bioinspired structures and material by using traditional manufacturing approaches such as molding,[25] femtosecond laser texturing, plasma nanotexturing, chemical vapor deposition (CVD), and nano-coating[26,27–29] However, there are several limitations in the traditional design and manufacturing of bioinspired interfacial structures in terms of geometry complexity, material selection, and controllable wettability.[24] Additive manufacturing provides a potential solution to reproduce biological intrinsically multiscale structures and multimaterial systems for interfacial applications.[24] Over the past thirty years, the manufacturing community has been benefitting from 3D printing, thanks to its capability of fabricating complex geometry from computer-aided design (CAD) models.[30] The principle of 3D printing is quite simple. Basically, a 3D digital model is first sliced into a set of 2D layers, and the material is accumulated layer by layer to form the 3D shape.[31] Recently, a lot of efforts have been made to develop a new 3D printing process to fabricate different materials.[32–34] According to the way layers of material are deposited to create 3D objects, 3D printing processes can be divided into seven categories: vat photopolymerization, material jetting, binder jetting, powder bed fusion, material extrusion, directed energy deposition, and sheet lamination.[30] Currently, different kinds of 3D printing technologies, such as two-photon polymerization (TPP), stereolithography (SLA), direct ink writing (DIW), extrusion-based 3D printing (EBP), and fused deposition modeling (FDM), have been used to build bioinspired multi-scale, multi-material and multi-functional structures for interfacial applications.[24,35,36] The advantages and disadvantages of common 3D printing technics are illustrated in **Table 1**. Because of the precise control of printing quality, 3D printing facilitates the manipulation and fabricating of interfacial surfaces with bioinspired structures and materials.[37–39] Together with the current progress of 3D printing process development, numerous types of functional material systems have been investigated to mimic natural unique architectures.[39–42] Integration of 3D printing and bioinspired design methodology promotes advancements in the fabrication of functional material and structures for future functional interfacial surfaces, which will further lead to breakthroughs of various applications in various industrial areas, including

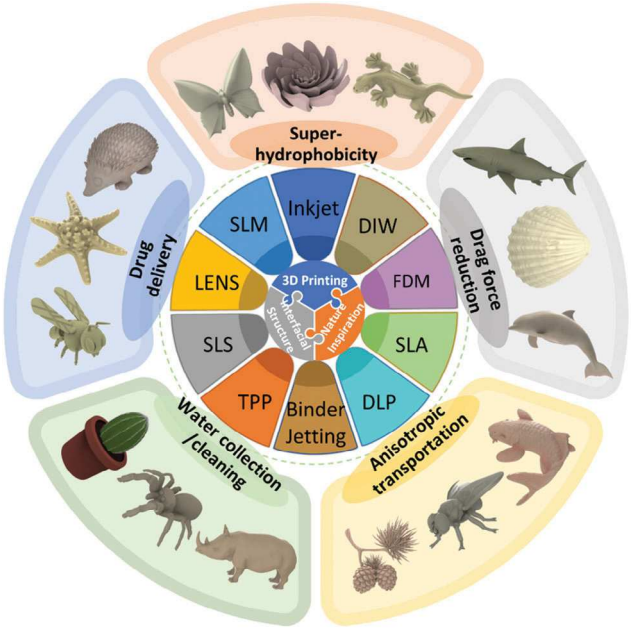

Figure 1. The interfacial functions and applications of 3D printing of biomimetic materials and structures. The reviewed applications include superhydrophobicity, drag force reduction, anisotropic water transportation, water harvesting and cleaning and drug delivery.

biomedical engineering, environmental engineering, chemical engineering, electronics, civil engineering, sustainable energy, etc.[2,24,38,43]

Bio-inspired structures, often derived from nature, exhibit a wide range of unique properties or characteristics. These properties can include, but are not limited to, superhydrophobicity, anisotropic liquid transport, drag force reduction, and more. Each of these properties can be thought of as distinct features that describe how these structures interact with their surroundings. What's important to understand is that these properties are not mutually exclusive. In fact, bio-inspired structures can possess multiple properties simultaneously. This means they can be both superhydrophobic and have anisotropic liquid transport capabilities, for instance. The combination of these properties can lead to structures that are highly adaptable and versatile. For example, a bio-inspired surface that is both superhydrophobic and has anisotropic liquid transport can be used for various applications, such as efficient water collection and enhanced oil-water separation. The superhydrophobic property repels water and contaminants, while the anisotropic transport property directs liquid flow in specific ways. This dual functionality makes the structure versatile, as it can serve different purposes in fields like water management, environmental cleanup, or oil spill mitigation.

Here, we summarized recent research works in the 3D printing of biomimetic materials and structures for interfacial applications (**Figure 1**). The revolution of 3D printing and functional material has brought us many opportunities to produce bioinspired interfacial structures. According to the interfacial functionalities, this paper is focused on five research topics in the field of interfacial science: (1) 3D printing of biomimetic superhydrophobic structures. (2) 3D printing of biomimetic structures for drag force reduction. (3) 3D printing of biomimetic structures for anisotropic water transportation. (4) 3D printing of biomimetic structures for water harvesting and cleaning. (5) 3D printing of biomimetic microneedles for drug delivery. In each aspect, the investigation of morphologies and internal mechanisms of biological structures are presented first. Afterward, the recent status of bioinspired design and 3D printing technology are discussed. Finally, the current achievement, existing challenges, applications, perspectives, and outlook of future potential works in each topic are put forward.

2. 3D printing of Bioinspired Interfacial Structures with Superhydrophobicity

2.1. Nature Inspirations for Superhydrophobicity

The design and development of newly various devices have been profoundly influenced and inspired by nature-existed creatures that have unique surfaces with specific functions.[1,44–48] At present, with the rise of biomimetic study, large amounts of nature-inspired structures have been fabricated and applied via the following natural concepts and design principles.[14,49–56] Specifically, superhydrophobic structure attracted lots of interest due to its wide applications, such as water-harvesting, oil/water separation, and droplet manipulation.[49,57–64] To understand superhydrophobicity, the surface with a water contact angle (CA) exceeding 150°can be defined as a superhydrophobic surface.[65,66] Presently, representative superhydrophobic surfaces have evolved in plants, animals, and insects. Particularly among plants, in **Figure** 2a, lotus leaves with papillae structure have become a symbol of superhydrophobicity, which even led to the concept of the 'lotus effect'.[67] The excellent CA of the lotus relied on the shape and density of the papillae. To compare the 'Lotus effect', the 'Petal effect' was also demonstrated as petals' surfaces of red roses (Figure 2b) have hierarchical micro-papillae and nano-folds which provided a sufficient roughness for superhydrophobicity.[68] Additional research by Barthlott et al, discovered that floating leaves of *Salvinia* were able to retain a layer of air when underwater (Figure 2c) .[16] This is because the hair structures in the leaf surface formed dense egg-beater structures covered with wax crystals, creating a nanoscale roughness for superhydrophobicity, which achieved a new concept as '*Salvinia Effect*'. These plant-based effects bring interesting perspectives for designing artificial surfaces with dense bulged structures and nano-level roughness to achieve superhydrophobicity. Figure 2d,e shows insect-inspired structures.[69,70] These surface structures displayed weak to strong hydrophobic properties, which were mainly dependent on slight changes in nanoscale shape and composition of the wax layer, offering an understanding of the diversity of the nanostructures. To further investigate, the adhesive force toward water is also significant for the superhydrophobic surface to achieve multifunctional applications. Multiscale structures play a key role in functional integration. Liu discovered gecko foot (Figure 2f) with a multiscale structure was capable of gaining both superhydrophobicity and a high adhesion towards water due to high-density nanopillars and could be considered a mechanical hand.[71] It brings more

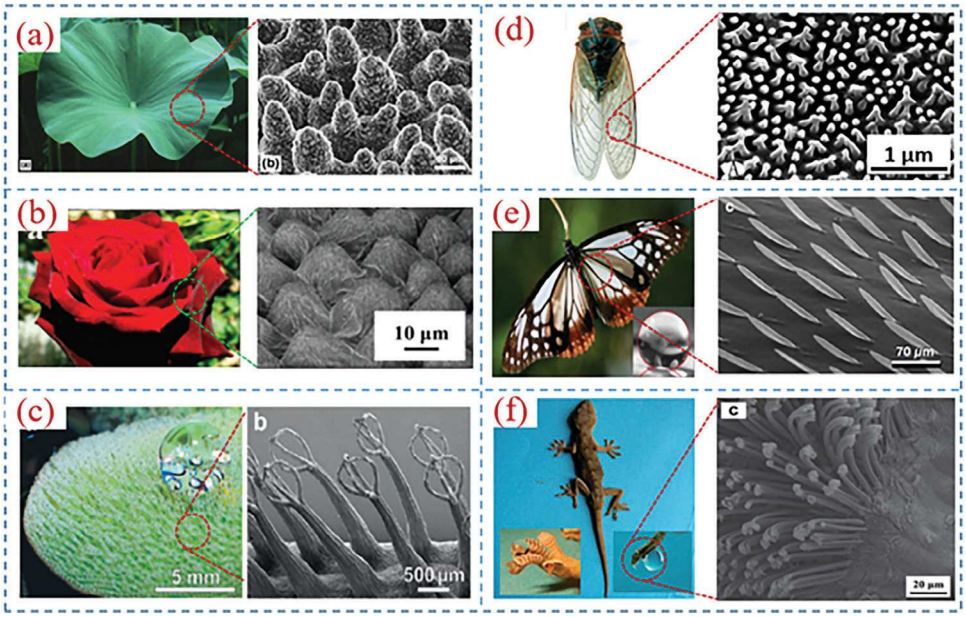

Figure 2. Bioinspired superhydrophobic surfaces. a) lotus leaf. Reproduced with permission.[67] CC BY 2.0. b) Red rose petal. Reproduced with permission.[68] Copyright 2008, ACS Publications. c) *Salvinia* leaf. Reproduced with permission.[16] Copyright 2010, Wiley-VCH. d) Cicada wing. Reproduced with permission.[70] Copyright 2009, The Company of Biologists Limited. e) Butterfly wing. Reproduced with permission.[69] Copyright 2009, Springer Nature. f) Gecko foot. Reproduced with permission.[71] Copyright 2011, Royal Society of Chemistry.

possibilities in the design of next-generation superhydrophobic surfaces to realize multi-applications.

2.2. Traditional Manufacturing Approach and Challenges

To apply the nature-inspired superhydrophobic structure, various fabrication strategies have been developed and utilized. Traditional methods include laser beam machining, hydrothermal growth, and molding.[25,72–75] For instance, Maghsoudi et al. reported using a compression molding method to fabricate superhydrophobic high-temperature vulcanized (HTV) silicone rubber with micro-nano structures on the surface.[75] The fabricated rubber showed a water contact angle above 160°, freezing delay, and ability to self-cleaning. These methods are able to produce superhydrophobic structures with stable mechanical properties. Nonetheless, with the large demands and rapid development of superhydrophobic surface for various applications, the fabricated surface require a denser structure, nano-scalar size, and complex structure. Therefore, previous fabrication methods have shown their limitations including tedious processes, high cost, and long-time fabrication. For example, fabricating a superhydrophobic surface on metal by laser ablation and electrodeposition method required a long sequential fabrication process, which contained laser beam machining, insulation, mechanical polishing, electrochemical deposition, and cleaning.[73] To overcome these challenges, 3D printing techniques with the high efficiency and capability of fabricating complex and micro-structures have been applied to replace the traditional fabrication methods to produce superhydrophobic structures for various applications, such as eggbeater structures for oil/water separation.[76–79]

2.3. 3D Printing of Bioinspired Superhydrophobic Structures

The structural design principles underlying superhydrophobic surfaces are rooted in a combination of microscale and nanoscale features that work synergistically to create surfaces highly repellent to water. These principles include the introduction of microscale roughness, often in the form of microstructured patterns, which increases the apparent contact angle of water droplets and minimizes the contact area. The hierarchical combination of these micro-nanostructures is a hallmark of superhydrophobic design, with the microscale features providing stability, while the nanoscale elements contribute to low adhesion forces, resulting in water droplets rolling off the surface with remarkable ease. At the microscale, surface roughness, often in the form of structured patterns or textures, plays a crucial role by increasing the apparent contact angle of water droplets, reducing the contact area, and promoting water repellency. On a nanoscale level, the incorporation of nanostructures or nanocoatings with low surface energy properties, such as hydrophobic materials, further enhances the water-repellent nature of the surface. The hierarchical combination of microscale and nanoscale features is a hallmark of superhydrophobic design, where microscale elements provide stability, and nanoscale features contribute to low adhesion forces. This synergy results in water droplets effortlessly rolling off the surface. Understanding and optimizing these structural features are key to creating effective superhydrophobic surfaces with applications in self-cleaning, antifouling, and microfluidic systems, among others. With the benefits of efficiency, higher resolution, and the ability to produce intricate and tiny structures, 3D printing technology plays a key role in the fabrication of various nature-inspired superhydrophobic surfaces.[44,49,80] The various complex pillar structures can be

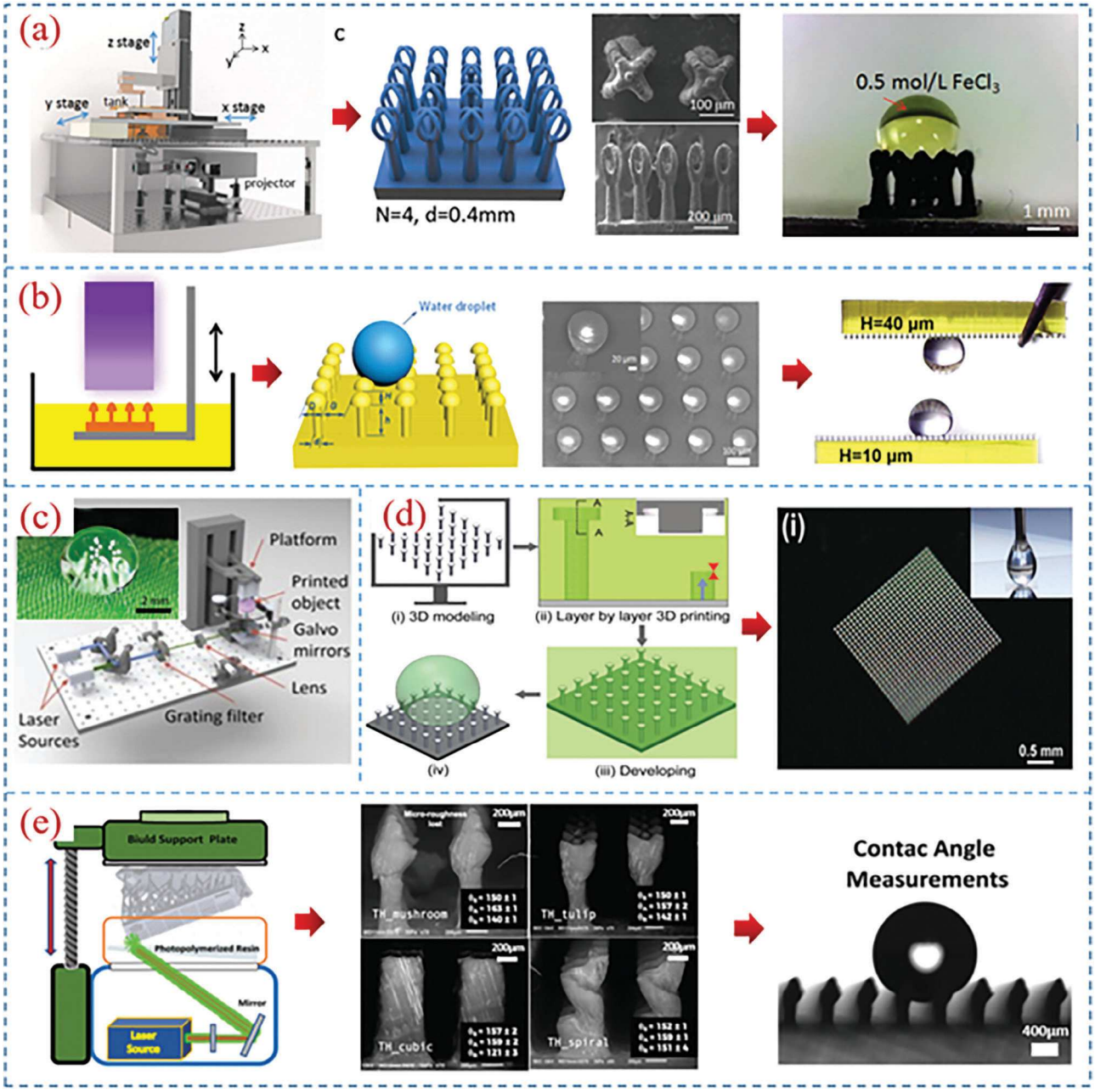

Figure 3. 3D printing techniques to fabricate superhydrophobic structures. a) Immersed surface accumulation-based 3D printing technique. Reproduced with permission.[49] Copyright 2017, Wiley-VCH. b) projection micro-stereolithography based 3D-printed method. Reproduced with permission.[81] Copyright 2021, ACS Publications. c,e) SLA techniques. Reproduced with permission.[82,84] Copyright 2019 and 2021, Wiley-VCH, and Royal Society of Chemistry. d) Two-photon polymerization-based 3D printing technology. Reproduced with permission.[83] Copyright 2018, Wiley-VCH.

designed, simulated, and then printed by 3D printers. Therefore, 3D printing superhydrophobic surfaces have become an attractive area of research. In a previously reported study, Yang et al demonstrated utilizing immersed surface accumulation-based 3D (ISA-3D) printing technique to print photocured epoxy mixed with carbon nanotubes to fabricate eggbeater structures inspired by *Salvinia* leaf, which showed an enhanced mechanical strength, obviously superhydrophobicity, and controllable adhesive force (**Figure 3a**) .[49] The printed surface also exhibited an extraordinary oil/water separation application. Besides, the 3D-printed micro-surface structures by using high-resolution resin also achieved dense arrangements and superhydrophobic properties.[56] In other work in this field, a projection micro-stereolithography (PμSL) based 3D-printed method (Figure 3b) was applied to print a mushroom-like surface with a contact angle (CA) of 171°.[81] Interestingly, The CA and adhesive force of the surface can be controlled by altering the geometric parameters of the printed surface, such as the interval distance,

Table 2. A comparison of the 3D-printed bioinspired interfacial structures with superhydrophobicity.

Material	3D Printing Method	Resolution	Bioinspired effect	Properties	Application	Reference
E-glass with MWCNT	ISA	35 μm	Super-Hydrophobic	Carbon nanotubes increase the modules 3 times	Microsample analysis	[78]
Methacrylated oligomers	Stereolithography	40 μm	Controllable hydrophilicity and hydrophobicity	Superior flexibility	Microreactor and droplet manipulation	[81]
SI-500	Stereolithography	40 μm	Super-Hydrophobic	Not mentioned	Not mentioned	[82]
Fluorinated solvents	Two-photon polymerization	10 μm	Super-repellence to water	Extreme low surface energy	Microfluidic device	[83]

height, and diameter of the mushroom's head and stalk, showing promising applications in droplet-based microreactors and droplet-based bio-detection. Furthermore, additional research by Li et al also demonstrated a multiscale stereolithography method with a maximum resolution of 37 μm was studied and applied to produce macroscale objects with microstructures and high throughput.[82] An artificial lotus leaf (Figure 3c) with micropillars and CA 139° was fabricated by a developed SLA process, showing an easily fabricated process. Another representative work for printed bio-inspired structures with outstanding water super-repellence was achieved by two-photon polymerization-based 3D printing technology.[83] In Figure 3d, printed structures were designed and simulated via the SolidWorks software. Micro open capillaries were built on the 3D-printed triply re-entrant array structures to implement directional spreading of liquid. Developed structures enable printing on stretched or solid platforms and can even still maintain the liquid super-repellence after the oxygen plasma process. Hence, combining bioinspired superhydrophobic structure and 3D printing methods are capable of achieving more complex structures and multifunctional applications. Since microstructures with roughness scales are of great significance for the application of superhydrophobic surfaces, recently, Bonilla-Cruz et al demonstrated they achieved using a scalable process to fabricate 3D printed microstructures with a dual roughness scale via stereolithography (SLA) technique (Figure 3e) .[84] Several designed pillar array structures were fabricated and printed via the SLA method at two orientations and three resolutions, which would bring more enhancements and possibilities in scalable and high throughput roughness design of the 3D printing superhydrophobic structure for various practical applications in the future. **Table 2** illustrates the comparison among the 3D-printed superhydrophobic structures.

2.4. Applications of 3D Printed Bioinspired Superhydrophobic Structures

In **Figure 4a**, the utilized printing techniques, printed materials, and printed resolution investigated in this section are listed and shown. And the summarized nature-inspired superhydrophobic structure including plant, animal, and insect-inspired

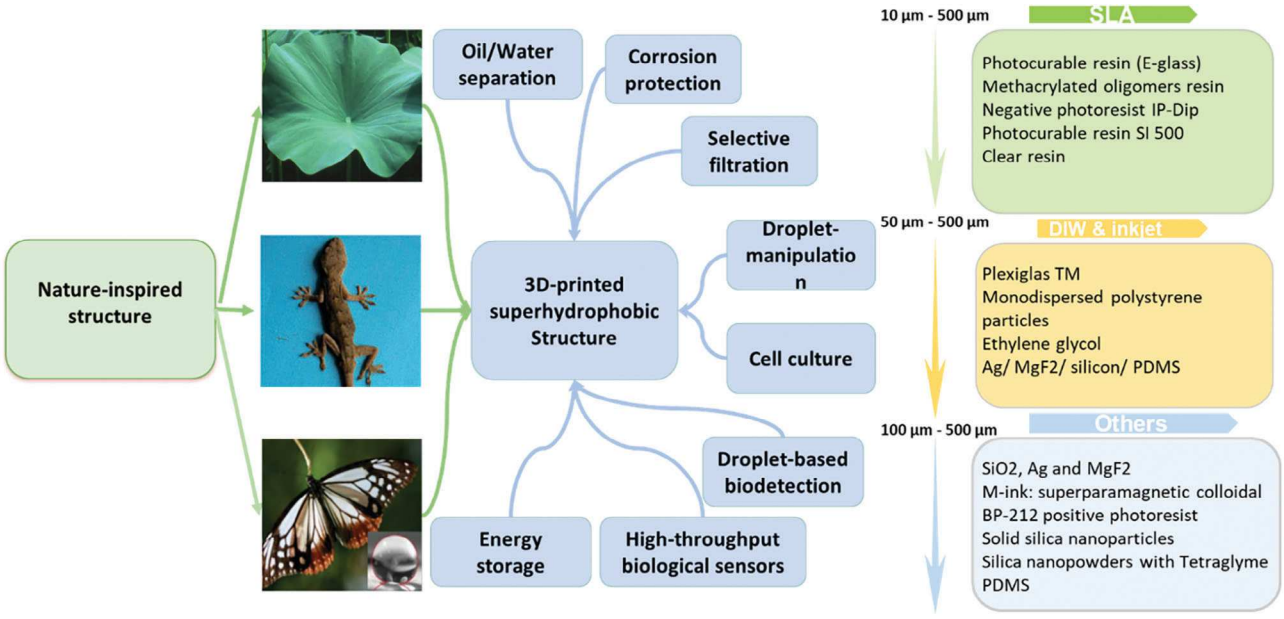

Figure 4. Summary of application of 3D-printed superhydrophobic structure.

structures, and their specific potential applications are demonstrated in Figure 4b. Based on the investigation, it is shown that the selection of the printed material needs to be further expanded. The properties of the printed sample including mechanical strength, thermal expansion, and biocompatibility, will be restricted by the single limited printed material, which will further hinder the further applications for 3D-printed superhydrophobic structures. Moreover, the structure design of the nature-inspired surface is simplistic. In previous works, the printed surfaces were replicated pillars, hence, leading to the fixed superhydrophobicity. In the future, the design of the advanced superhydrophobic structure will combine multiple nature-inspired pillar structures to achieve multiple superhydrophobicity to gain multifunction. Additionally, with the fast development of bioelectronics, the potential applications of the 3D-printed superhydrophobic surface, such as energy storage, droplet-based bio-detection, and high-throughput biological sensors, need to be deeply studied in the future.

3. 3D Printing of Bioinspired Interfacial Structures with Drag Force Reduction

The characteristics of natural creatures have provided numerous inspirations to humans in solving global engineering problems. This section highlights the design and principles of the natural structure for drag force reduction, the traditional manufacturing approaches for drag force reduction, and briefly summarizes the encountered challenges during manufacturing, and highlights the benefits of 3D printing and applications of printed drag force structures.

3.1. Nature Inspirations for Drag Force Reduction

Drag force reduction refers to the resistance force of a body moving in a fluidic environment. The reduction in surface friction resistance results in low energy consumption for moving bodies.[85] There are two common types of drags involved in drag reduction such as pressure and friction drag which affect the movement of objects in a fluidic environment. The pressure drag is due to a change in the pressure in the front and rear of a moving object. On the other hand, friction drag is caused by the attraction of the fluid molecules to the surface of the moving object.[10] As a result, viscous fluids exhibit greater drag compared to less viscous fluids, and the fluid layers in direct contact with the surface of an object are commonly referred to as boundary layers. The boundary types are measured using the Reynolds number (Re) which is the ratio of the inertia forces to viscous forces = density*fluid velocity*length/dynamic viscosity. There are two types of boundary layer flow laminar and turbulent flow, the laminar flow with Reynold's number lower than 2300 is smooth while the turbulent flow is chaotic which causes the increased friction to drag because of increases in the momentum of the fluid.[10]

The study of drag reduction has attracted extensive interest because of its potential impact on future developments.[86] Different research has been conducted to discover the unique drag reduction ability of natural structures, such as the sharkskin, dolphin, sailfish, paradise fish, filefish, Carassius auratus fish, lotus leaf, rice leaf, and nepenthes alata. Those structures' drag reduction properties would be implemented in modern society such as submarines ships, airplanes, water and oil pipelines transportation, manufacturing of swimming suits, windmills, high-speed trains. Nature organisms possess abilities to help researchers imitate the drag reduction process. One of the good examples is the shark skin drag reduction mechanism in **Figure 5a**. The sharks are best known as fast swimmers, which is due to the presence of the dermal riblets, and mucus presence on the sharkskin which enhances their drag reduction.[87] The dermal riblets scale from 0.2 mm to 0.5 mm which is in the direction of flow as such reduces the turbulent effects and momentum and shear stress on the surfaces and reduce surface exposure to the high velocity as a result of the drag reduction on the riblets surfaces.[88] Additionally, sharkskin drag reduction depends on the attacking angle for sharkskin scale which can vary with the direction of fluid flow, and the mucus increases the viscous layers on the sharkskin surface as such reduce turbulence.[89] The Cetacea dolphins shown in Figure 5c have been considered as one of the fastest swimmers due to their drag force reduction.[90] Additionally, the ability of the dolphin to change the skin muscle also impact their response to drag reduction.[91] The orca and dusky dolphin show significant drag reduction by 7% based on the color change of the dolphin.[92] Lotus leaf is a superhydrophobic material that can reduce drag due to slip and air-water interface on the leaf surface.[93] The sailfish in Figure 5b uses the mucus on the fish scales to reduce drag.[94] Most aquatic animals such as paradise fish shown in Figure 5d, filefish in Figure 5e, and puffer fish shown in Figure 5f possesses scales and mucus on the surface which have shown effects on drag reduction.[95–98]

3.2. Traditional Manufacturing Approach and Challenges

There are various manufacturing processes used to imitate the drag force reduction surfaces such as traditional methods (**Figure 6**). There are six traditional methods such as direct bio-replicated micro-imprinting technology,[99] synthetic fabricating, bio/macro rolling, solvent-swelling proportional shrunken, UV curable painting, and stretched deforming. The traditional methods have limitations such as manufacturing complex riblet structures, increased manufacturing costs using polymer extrusion, and lithography.[100] The lithography method was used to generate the nanostructures in production and analysis of metallic riblet structure through mimicking the skin of mako shark.[100] Additionally, the laser engraving and polishing were also used to manufacture the biomimetic fish structures.[101] The bio-replicated rolling method was mainly used to estimate the drag reduction effect of the water tunnel after the sharkskin was glued together with 704 silicon rubber to form a sharkskin roller while the UV curable painting was mainly used to form a large roll shark bionic surface with more drag reduction in comparison to the double dimensional riblet.[102] The direct-replicated shark skin method indicated that the coated sharkskin surfaces influence drag reduction on large surfaces.[102] The study showed that the biomimetic sharkskin surfaces would provide great wet performance.[103] Furthermore, the direct bio-replica method results in great quality and good drag reduction effects of biomimetic sharkskin surfaces before curing, the

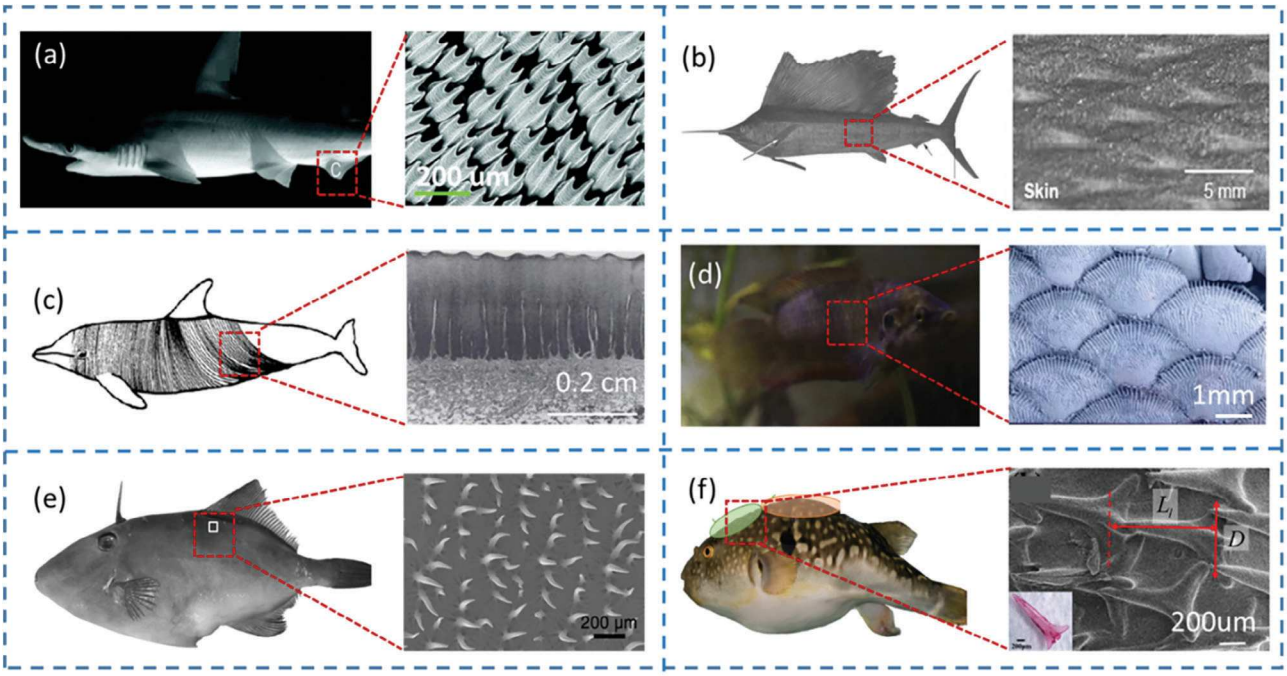

Figure 5. Nature drag reduction structure. a) Shark skin. Reproduced with permission.[87] Copyright 2014, Company of Biologists limited. b) Sailfish. Reproduced with permission.[94] Copyright 2013, CC BY 3.0. c) Dolphin. Reproduced with permission.[90] Copyright 2017, IOP Publishing. d) Paradise fish. Reproduced with permission.[95,96] Copyright 2019 and 2020, Elsevier and Cambridge University Press. e) Filefish. Reproduced with permission.[98] Copyright 2014, Wiley-VCH. f) Puffer fish. Reproduced with permission.[97] Copyright 2021, ACS Publications.

replicated shark skin surface was treated with UV light to improve the skin resolution.[99,102] The bio replicated squalus anthias shark skin indicated pressure drops under laminar and turbulent flows with an increase in pressure drops leading to an increase in viscous drag due to air in the denticles.[104] However, the main challenges of using the traditional printing methods were time and energy consumption.

3.3. 3D Printing of Bioinspired Structures for Drag Force Reduction

Various 3D printing methods and techniques are used to manufacture the drag force reduction surfaces to reduce the costs, energy consumption and time in the traditional approaches.[105] For instance, the vinyl-film riblets are easiest to manufacture and save time during manufacturing processes.[10] The additive manufacturing or 3D printing methods has provided alternative ways to generating cost-effective products, saving time, and producing highly complex shapes both on micro and nanoscale level. To manufacture biomimetic drag force reduction structures, different 3D printing methods are used such as stereolithography, fused deposition modeling (FDM), and x-ray microtomography.

Stereolithography (SLA) was used to solve the challenge of throughput and resolution, this process used laser beam to print pipes with shark skin inspired features to be used in pressure flow analysis in the pipe. The stereolithography process use lasers with 405 nm and 445 nm wavelength and the cross-section view of four pipes have different interior textures. This was used to compare the friction factors for the smooth pipe with 142 μm shark skins micro riblet features.[82] Besides, the 3D printed shark skin denticles structures for hydrodynamic testing using plastic foil was also achieved.[87] The Shark skin structures were printed by scanning the shark skin denticles from Isurus oxyrinchus using the multimaterial 3D Printing based on the micro-computed tomography(micro-CT) .[105] In this process, the plastic foils were made by laser cutting plastic shim stock material with a thickness of 0.508 mm and glued together with synthetic sharkskin to form a sandwich to be used in testing the hydrodynamic. Another fabrication method used was the Flash Forge Dreamer Dual Extrusion 3D printer for 3D printing shark skinned denticles structures with thickness range (100 μm – 400 μm) in different scale orientations from smooth, parallel, mix and perpendicular (Figure 6a) .[106] In this process the used material is acrylonitrile butadiene styrene (ABS). The orientation of printed shark skins was to analyze the fluid viscosity on the surface where the velocity is low at the center while the edges have highest velocity in the parallel oriented shark skin structures as such has high drag reduction. The perpendicular orientation indicated low velocity gradient which indicated less required energy to change momentum between fluid and the surface because lower viscosity and drag reduction.[106] Figure 6b indicates the 3D printing of the shark skin structures with different denticle patterns and spacings, such as staggered-overlapped, linear-overlapped, and linear non overlapped. The process was to analyze effects of denticle pattern and spacing on the hydrodynamic function of biomimetic shark skin. The printed models' stationary and dynamically movements were

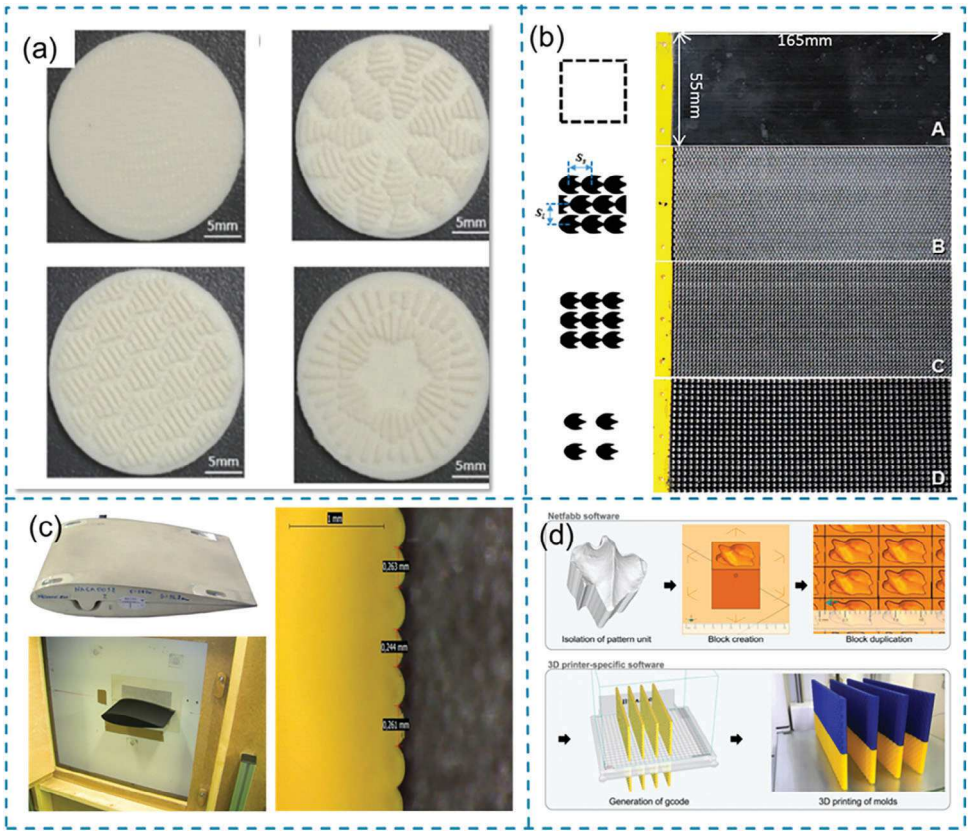

Figure 6. 3D printing of shark skin denticles. a) 3D printed shark skinned surfaces with different scale orientations such as smooth, parallel, mix and perpendicular. Reproduced with permission.[106] Copyright 2019, CC BY 4.0. b) Hydrodynamic function of biomimetic shark skin: effect of denticle pattern and spacing. Reproduced with permission.[107] Copyright 2015, IOP Publishing. c) Application of FDM technology to reduce aerodynamic drag. Reproduced with permission.[109] Copyright 2019, Emerald Publishing Limited. d) Manufacturing of biomimetic silicone rubber films for experimental fluid mechanics. Reproduced with permission.[110] Copyright 2019, CC BY 4.0.

tested in the flow tank with a mechanical flapping device. As such the static tests indicated the drag reduction in denticle patterns with staggered-overlapped pattern demonstrated the high swimming abilities.[107] 3D printed Marko shark (Isurus oxyrinchus) skin denticle is manufactured using layer-by-layer 3D printing technology and two-photon lithography with the synthetic shark structure designed and fabricated by Wen et al. The denticle model of a male shortfin mako shark was generated using the 3D modeling software and membrane was analyzed in SolidWorks, and after 3D printing the membrane distribution, spacing, size and overlapping were obtained as they appeared on the natural Marko skin.[108] The 3D printing method was used because of its flexibility and reproducibility abilities in manufacturing drag reduction structures which made it possible to see and analyze the denticle arrangements, shapes, size and textures in all directions. Another manufacturing method used is FDM technology to reduce the aerodynamic drag as shown in Figure 6c. In this process the thermoplastic polymer filament such as 0.178 mm of acrylonitrile-butadiene styrene (ABS), 0.254 mm of polylactic acid (PLA), and 0.330 mm of polycarbonate (PC) were used.[109] In Figure 6d indicates the use of the x-ray microtomography in 3D printing the shark skin mold using the polylactic acid (PLA) at 60 µm resolution in manufacturing of biomimetic silicone rubber films for experimental fluid mechanics.[110]

3.4. Applications of 3D Printed Bioinspired Drag Force Reduction Interfaces

In **Figure 7**, the utilized fabrication methods, selected materials, and potential applications for 3D printed drag force reduction surfaces are listed and exhibited. The printed surfaces can be applied in gas pipeline, airplane, ship, racing car, swimming suit, windmill, golf ball, and high-speed train. Also, they have different benefits in solving everyday challenges in various sectors such as sharkskin scales being used to reduce the sailing resistance. Additionally, 3D printed denticles would reduce the energy and sharkskin riblets structures are used to make swimsuits and airplanes geometries. The drag reductions resulted in savings of fuel in the flight.[10] Nevertheless, bionic microstructures can have contrasting effects on drag force depending on their specific design and application. Some microstructures, inspired by nature, are engineered to reduce drag and enhance hydrodynamics, leading to improved efficiency and performance in applications like transportation and sports. Conversely, in other cases, microstructures may increase drag but offer advantages such as enhanced adhesion, anti-fouling properties, or precise control in microfluidics. In microfluidic devices, artificial cilia or microstructures inspired by cilia are used to manipulate fluids. These structures can generate fluid flow or transport

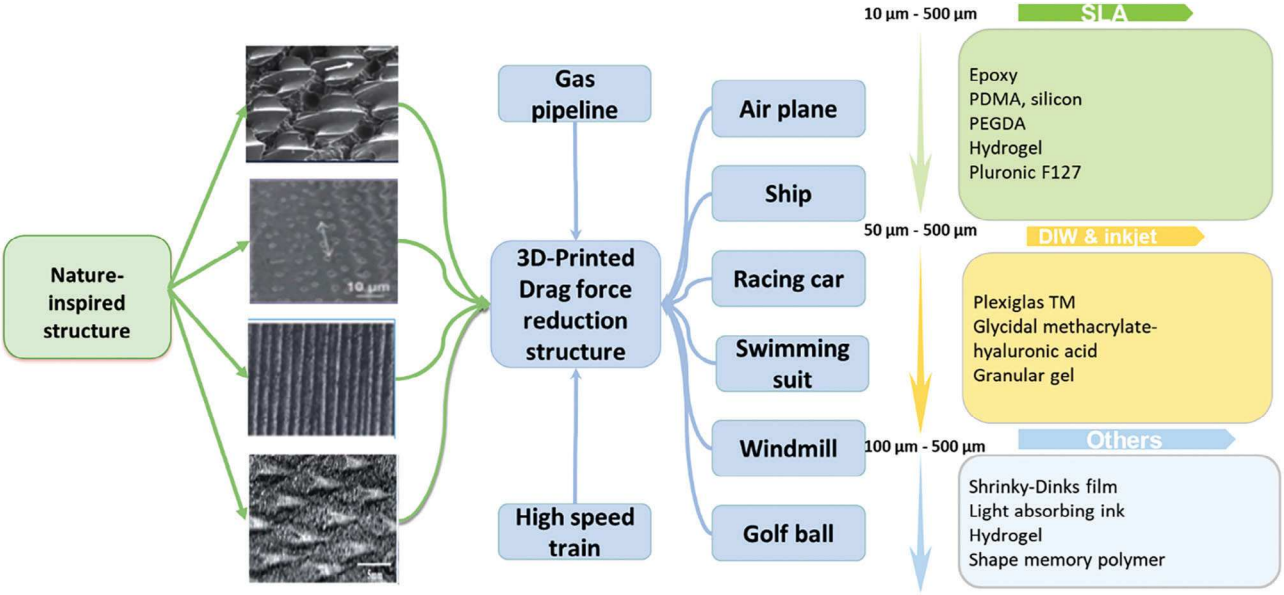

Figure 7. Summary of application of 3D-printed drag force reduction surfaces.

particles. However, in some cases, the microstructures may create more drag, affecting the efficiency of fluid transport. Still, this increased drag can also enhance mixing and control in microfluidic systems. The 3D-printed microfluid will be discussed in detail in the following sections. The choice of microstructure and its impact on drag force depends on the desired outcomes and the context of the application. Drag reduction structures are used in everyday modern society applications such as submarines ships, airplanes, water and oil pipelines transportation, manufacturing of swimming suits, windmills, high-speed train. However, there are challenges in processing and manufacturing those structures. The 3D printing technology approach will solve those challenges, and more research work is needed in the fluid reduction field to explore natural behaviors in finding world challenges.

4. 3D Printing of Bioinspired Interfacial Structures with Anisotropic Liquid Transport

4.1. Nature Inspirations for Anisotropic Liquid Transport

Many organisms in nature have evolved anisotropic microstructure surfaces to achieve anisotropic water transport, which is vital to their survival.[111–114] For example, the millimeter-level 3D ratchets on the surface of Araucaria leaves allow liquid to flow to the inner and outer sides of the ratchet plane under capillary force.[115] The gradient wet synovial membrane on the surface of the Nepenthes peristome leads insects to slip and fall into the pitcher cage and be preyed once they land on the mouth margin.[116] The unidirectional driving characteristic of the droplet on the surface with anisotropic structure is determined by the non-uniform surface potential energy. When the droplet contacts the anisotropic surface, the surface curvature of different positions causes the surface potential energy gradient. Then the droplets are moved by the Laplace pressure difference.[117,118] The research on the anisotropic transport of droplets on the natural structure surface allows us to understand the principles behind and provides insights for the design of anisotropic water transport surfaces, which play a key role in the fields of microfluidic devices, biomedicine, and droplet manipulation.

For a long time, it has been believed that the liquid on the substrate surface tends to flow in the direction of decreasing surface energy. The flow direction mainly depends on the surface structure and has nothing to do with the properties of the liquid itself such as surface tension. However, the latest research found that liquids with different surface tensions spread in completely opposite directions on the *Araucaria* leaves (**Figure** 8a), which are composed of many ratchets arranged regularly and inclined to the tip of the leaf.[115] The ratchet allows the liquid to determine its direction of diffusion based on the interaction between its surface tension and structure surface. For liquids with high surface tension like water, they flow in the opposite direction against the inclination of the ratchet. In contrast, for low surface tension liquids like ethanol, the flow is in the opposite direction. Different from previous studies, the solidified lipid matrix covered by the regularly arranged scales on the snake body not only has high lubricity and wear resistance, but also plays an important role in anisotropic liquid transmission. *Lampropeltis pyrmelana* (Figure 8b), whose ventral skin is evenly covered with a hydrophobic lipid layer, has a low contact angle hysteresis and periodic hierarchical wrinkles, and shows low liquid adhesion loss and a large amount of water transport capacity.[119] As water is continuously supplied to the scales, the volume of the droplets continues to increase, but the diffusion of the droplets stops at the back edge of the scales and only spread forward. The directional transmission characteristic is attributed to the coupling effect of topological reciprocation and liquid bridge effect. To keep the body dried in a highly humid living environment, the drain fly (Figure 8c) has evolved an outstanding drainage solution.[120] Since the condensate droplets

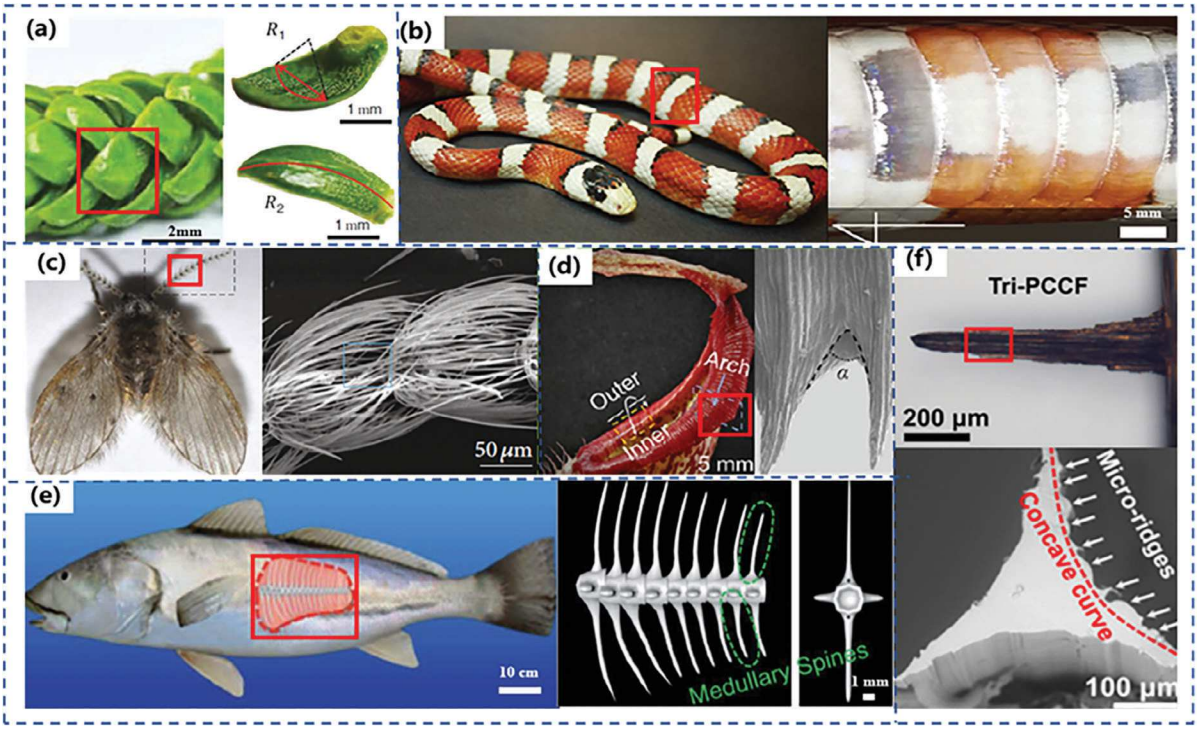

Figure 8. Structures for anisotropic water transport. a) *Araucaria* leaf. Reproduced with permission.[115] Copyright 2021, The American Association for the Advancement of Science. b) *Lampropeltis pyromelana*. Reproduced with permission.[119] Copyright 2020, Wiley-VCH. c) Drain fly. Reproduced with permission.[120] Copyright 2020, CC BY 4.0. d) *Nepenthes*. Reproduced with permission.[121] Copyright 2020, CC BY 4.0. e) fish medullary spines. Reproduced with permission.[122] Copyright 2021, Royal Society of Chemistry. f) P-concave curved-fiber. Reproduced with permission.[123] Copyright 2020, ACS Publications.

continuously coalesce and are transported in a directional manner, the body of the drain fly maintains high hydrophobicity. Water vapor initially randomly condenses into tiny droplets in a single knot on the surface of the tentacles. As time goes by, the growing droplets reach the apex of a single bristle which is manifested by frequent coalescence with adjacent droplets. The droplets are guided between the individual parabolic knots to coalesce, after which all condensed droplets are effectively transferred to the end of the tentacle and finally removed.

Living in a nutrient-poor and high-humidity environment, *Nepenthes* (Figure 8d) constructs a slippery peristome to trap insects to obtain a source of nitrogen.[121] Numerous studies have proved that the directional transmission of the smooth water layer on the *Nepenthes* peristome is benefited from the micro concave array or arch structure. Utilizing the surface curvature of the ratchet, cavity and arched channel, the rim of the peristome continuously and quickly collects and transports condensate. Even if the tip of the peristome is pointing downwards, the Laplace pressure is increased in the ratchet teeth and cavity area, prompting the condensed droplets to be transported in the direction opposite to gravity. Furthermore, the synergistic action between adjacent ratchet teeth prevents the dripping of condensed droplets, and finally succeeds in pushing the collected water up at an ultrafast speed. Cui et al. observed an inspiring phenomenon of directional transportation of oil droplets from the tip to the base of the fish medullary spine (Figure 8e) .[122] Through systematic characterization and analysis, many pores on the surface of the spine are found. Furthermore, the different pore distribution densities in the two regions near the tip and base confirmed the presence of a structural gradient on the surface of the fish medullary spine from tip to base. Natural medullary spines have excellent transport capacity for droplets, which are attributed to the cone and porous structure. The test results show that natural medullary spines have excellent transport capabilities for droplets, which are attributed to the cone and porous structure. Inspired by the self-propelled directional liquid transport (SDLT) in nature, for example, spider silk can effectively capture water through its periodic spindle and joint structure,[18] and the spine of the cactus cone structure helps to efficiently collect water to survive in arid environment.[37] Hu et al. developed a unique P-concave curved-fiber (PCCF) (Figure 8f), which can realize ultra-fast SDLT.[123] The transmission direction of the liquid is determined by the Laplace pressure difference (FL) caused by the conical structure. Specifically, the SDLT on the surface of PCCF accelerates under the synergistic effect of the capillary rise caused by the concave surface and the oriented micro ridges/valleys and the enhancement of FL caused by the decrease of the cross-sectional area. It is believed that PCCF will open up a new perspective for the establishment of microfluidics and liquid manipulation systems.

4.1.1. Self-Propelled Droplet Transport on Structurally Anisotropic Surfaces

The structurally anisotropic surface exhibits a gradient wettability characteristic. When a droplet contacts the flat surface, the

contact angles at the left and right end of the droplet are different, resulting in an imbalance in the interface tension at ends of the contact line. The difference in interface tension drives the droplet to move to a position with lower surface tension. The tendency of the unidirectional movement can be expressed by the following formula[124]:

$$\vec{F}_{T,\mathrm{surf}} = \vec{\nabla}_{\mathrm{surf}}\sigma \tag{1}$$

where $\vec{F}_{T,\mathrm{surf}}$ is the tangential surface force, $\vec{\nabla}_{\mathrm{surf}}$ is the surface gradient, and σ is the surface tension. Furthermore, this unbalanced interface force, that is, the driving force of the wetting gradient, can be calculated as[117]:

$$F_d = 2E\gamma_{\mathrm{lg}}\int_0^{\pi/2}\left(\cos\theta_{\mathrm{A}} - \cos\theta_{\mathrm{B}}\right)\cos\phi \mathrm{d}\phi \tag{2}$$

where R is the base radius of the contact between the droplet and the interface, γ_{lg} is the liquid-gas interfacial tension, θ_{A} and θ_{B} are the contact angles of the droplets on the left and right sides of the wetting gradient respectively, ϕ is the polar angle, ranging from 0 to $\pi/2$.

Different from the planar wetting gradient, the conical surface has asymmetric structural characteristics. After the droplets wet the outer surface of the structure, the surface of the droplet spontaneously forms a liquid surface with different curvatures, and then moves directionally under the action of the difference in surface tension. The pressure difference directed towards the bottom of the conical structure is[125]:

$$\Delta p = -\int_{x_B}^{x_A}\frac{2\gamma_{\mathrm{lg}}}{\left(R + R_0\right)^2}\alpha \mathrm{d}x \tag{3}$$

x_{A} and x_{B} are the distances between the front and back ends of the droplet relative to the tip of the cone, α is the half apex angle of the cone, R_0 is the radius of the droplet and R is the radius of curvature of the cone. When the droplet is located inside the cone structure, the movement direction is closely related to the hydrophobicity (or contact angle) of the liquid, and the driving force caused by the asymmetric structure is[125]:

$$\Delta p = \frac{4\gamma_{\mathrm{lg}}\cos\theta}{x_B\alpha} - \frac{4\gamma_{\mathrm{lg}}\cos\theta}{x_A\alpha} \tag{4}$$

θ is the contact angle of the droplet on the solid surface. When $\theta < 90°$, the liquid surface is concave, and the droplet moves to the top of the cone. When $\theta > 90°$, the liquid surface is convex, and the droplet moves to the bottom of the cone.

4.1.2. Slippery Lubricant Impregnated Porous Surfaces

Inspired by the predation method of Nepenthes pitcher plants, Wong et al. first proposed slippery lubricant impregnated porous surfaces (SLIPS) .[126] Unlike the gas-liquid film on the superhydrophobic surface, the SLIPS produce a smooth, continuous and chemically uniform liquid-liquid surface by infusing various lubricants into micro-nano structures. The surface cannot be saturated by most of the liquid, showing a low contact angle hysteresis. Moreover, the lubricating film on the surface significantly reduces the roughness of the substrate surface, reduces the friction force when contacting with the droplets, and effectively avoids the disadvantages of pinning effect and the shortcomings of the slow droplet movement of the structurally anisotropic surfaces.[127–130] Three principles for constructing SLIPS were summarized: 1) The lubricant must penetrate into the substrate and be firmly adhered; 2) The lubricant can infiltrate the substrate material, and the chemical affinity between the substrate and lubricant must be greater than the chemical affinity between the substrate and the repelled test liquid; 3) The lubricant is insoluble with the repelled test liquid. Only by satisfying the above three conditions can a stable lubrication film be maintained.[126] The nano-composite rough structure on the surface and the good affinity between the surface and lubricant are the key factors to constructing SLIPS. At the same time, equations (5) and (6) need to be satisfied so that the solid can be preferentially wetted by the lubricant, otherwise the repulsive fluid may replace the lubricant and lay flat on the substrate surface.[126]

$$\Delta E_1 = R\left(\gamma_{\mathrm{B}}\cos\theta_{\mathrm{B}} - \gamma_{\mathrm{A}}\cos\theta_{\mathrm{A}}\right) - \gamma_{\mathrm{AB}} > 0 \tag{5}$$

$$\Delta E_2 = R\left(\gamma_{\mathrm{B}}\cos\theta_{\mathrm{B}} - \gamma_{\mathrm{A}}\cos\theta_{\mathrm{A}}\right) + \gamma_{\mathrm{A}} - \gamma_{\mathrm{B}} > 0 \tag{6}$$

where γ_{AB}, γ_{A} and γ_{B} represent the interfacial tension of the repelled test liquid-lubricant interface, the repelled test liquid-air interface and the lubricant-air interface respectively, θ_{A} and θ_{B} represent the equilibrium contact angles of the repelled test liquid and the lubricant with substrates respectively, and R is roughness ratio.

The methods of constructing SLIPS can be roughly divided into two categories: top-down and bottom-up.[131] The first type of method includes self-assembly or spraying, brush coating, etc., in which micron-nano TiO_2, SiO_2, and other particles are mixed into the coating to construct micro-nano structure, and then lubricating liquid is filled to obtain super-slippery surface.[132–134] The advantage of this type of method is that it can ignore the shape and size of the substrate, but it has the drawback of poor binding force. The second method is to directly construct the microstructure on the surface of the substrate by etching printing and filling it with lubricant to form the super-slippery surface.[135–137] Most of the super-slippery surface obtained by this method has high structural stability and strong durability.

4.2. 3D Printing of Bioinspired Structures for Anisotropic Liquid Transport

From the aforementioned transmission principle and structural characteristics of the anisotropic water transport structure, it is obvious that under the current situation of slow manufacturing speed, high cost, high equipment requirements, and small-scale production, the manufacture of the unidirectional droplet transport structure has unprecedented difficulties, especially involving the manufacture of emerging bionic structures. Traditional micro-nano surface structure

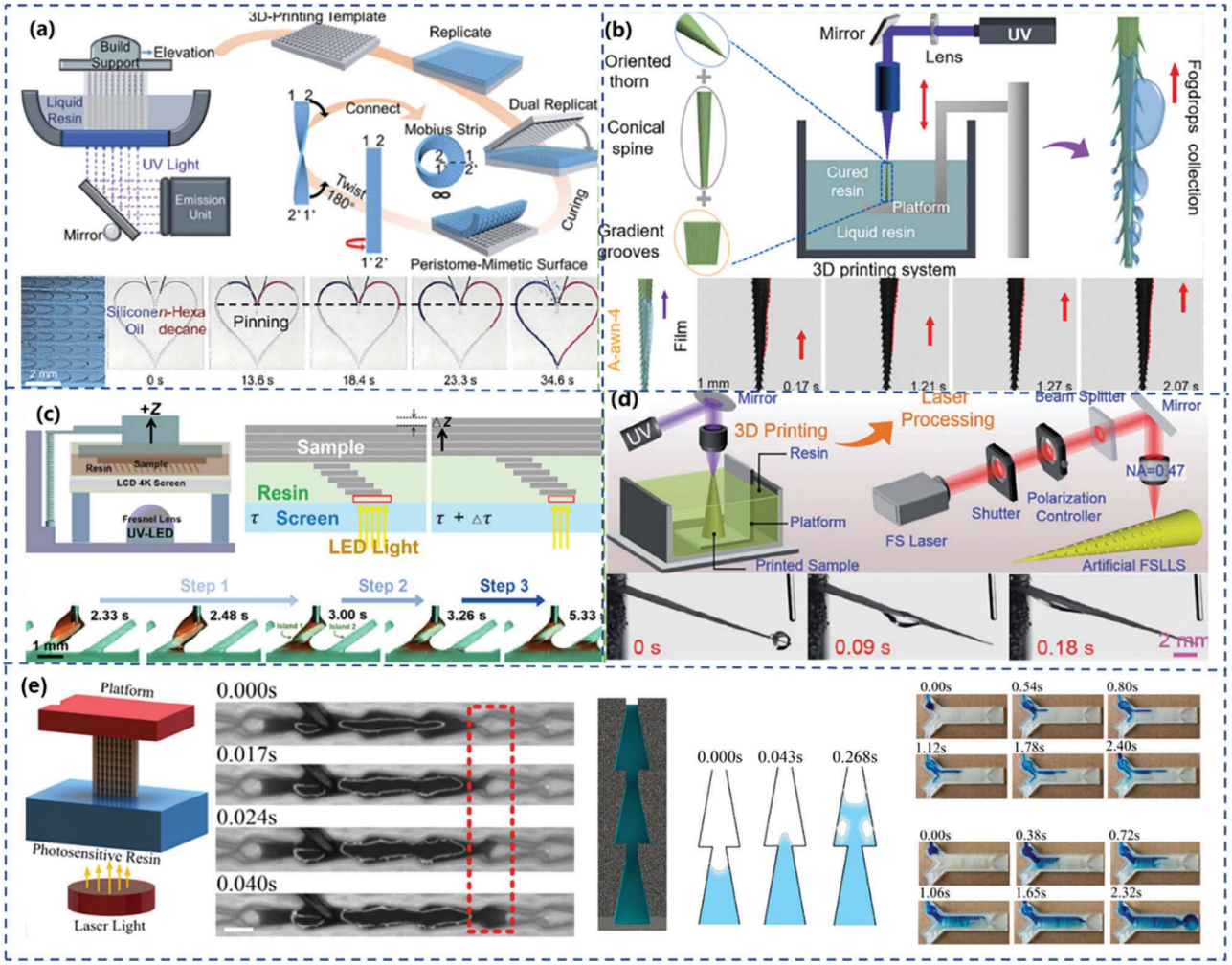

Figure 9. 3D printed structures for anisotropic water transport. a) Schematic demonstration of the manufacturing process of peristome-mimetic surface and unidirectional droplet transmission on the 2D curve. Reproduced with permission.[141] Copyright 2019, Royal Society of Chemistry. b) Diagram of the 3D printing process of the awn-mimetic systems and the anti-gravity droplet transport. Reproduced with permission.[142] Copyright 2020, Elsevier. c) Demonstration of the fabrication of the dual-scale A-shaped island arrays by DLP printing and the liquid transportation between two adjacent islands under overlapped Laplace pressure. Reproduced with permission.[143] Copyright 2018, ACS Publications. d) Schematic diagram of 3D printing and laser structuring process of the FSLLS and anisotropic oil transmission. Reproduced with permission.[122] Copyright 2021, Royal Society of Chemistry. e) Schematic diagram of photocuring 3D printing arrow and unidirectional water transport in arrow direction. Reproduced with permission.[145] Copyright 2019, CC BY 4.0.

preparation methods such as chemical etching, electrochemical deposition, sol-gel, and other methods are mainly used to produce isotropic micro-nano structure surfaces. However, with the continuous exploration of micro-nano structure preparation methods, the development of advanced manufacturing technology paths a new way for the manufacture of unidirectional droplet transport surfaces.[137] Femtosecond laser lithography has the ability to manufacture 3D micro/nanostructures quickly and efficiently.[138] Nanoimprinting transfers the micro/nano structure on the template directly to the surface to be processed with the assistance of photoresist.[139] It has a resolution exceeding that of traditional lithography technology. As a revolutionary manufacturing method, 3D printing has great potential in manufacturing unidirectional droplet transport structures.[140]

Zhou et al. used high-resolution stereolithography to fabricate a microcavity array substrate that can achieve the directional transmission of droplets by imitating the microstructure of the surface of the Nepenthes peristome (**Figure 9a**) .[141] First, the inverse mold is manufactured by 3D printing, and then PDMS or PVA is cast on the printed mold. Finally, the pseudo-peristome PDMS surface and the PVA hydrogel surface are obtained after curing and demolding. Furthermore, by performing topological transformation of the pseudo-peristome substrate, unconstrained unidirectional transmission in 1D linear, 2D curve and 3D infinite space is realized. Recently, the distinctive hierarchical structure and superior droplet collection capability of wheat awns were discovered by researchers. Xiao et al. used 3D printing technology to develop an artificial awn-like system with a hierarchical spine structure, which exhibited excellent droplet capture

Table 3. A comparison of the 3D-printed interfacial structures with anisotropic liquid transport.

Material	3D Printing Method	Resolution	Bioinspired effect	Properties	Application	Reference
1,6-hexanediol diacrylate (HDDA)	Projection Micro Litho Stereo Exposure	20 μm	Hydrophilic	The collection efficiency is 5.90 g cm^{-2} h	Potential device for fogdrops collection	[146]
VeroClear-RGD 810	DLP 3D printing	25 μm—100 μm	Hydrophobic	Transport dynamics at the speed of 1000 nL s^{-1}	Potential external energy supply	[143]
PVA hydrogel	DLP 3D printing	100 μm	Hydrophilic	Water elevation velocity can reach 43.5 mm $^{-1}$s	Self-siphon and siphon diode	[144]
Photosensitive resin	DLP 3D printing	100 μm—500 μm	Super-Hydrophilic	Liquid transport velocity can reach 23 mm $^{-1}$s	Micromixers	[145]

and rapid transmission capability (Figure 9b) .[142] The bionic hierarchical structure is composed of a tapered spine, gradient microgrooves and regularly arranged thorns. The vapor first condenses on the thorns into droplets and then transforms into a thin film on the spine driven by the difference of Laplace pressure and capillary force and continues one-way transportation. The test results show that the collection efficiency of the bionic system is 5.90 g cm^{-2} h, and the transmission speed of the four rows of thorns system is up to 3.5 mm $^{-1}$s. Si et al. utilized DLP to print a micro/macro dual-scale A-shaped island arrays that can transport liquids rapidly, spontaneously, and continuously in a single direction, which can drive liquid anti-gravity transportation only by relying on Laplace pressure difference without external energy input (Figure 9c) .[143] Dual-scale A-shaped island arrays have a high degree of manufacturing freedom, and can build microfluidic patterns, liquid splits and microfluidic devices like LEGO bricks, which is of great significance to the construction of labs-on-a-chip equipment, integrated microfluidic systems and biochemical microreactors.

Cui et al. found that the micropits on the surface of the fish medullary spines exhibit excellent anisotropy during liquid transportation and developed a fish-spine-like liquid splitter (FSLLS) with the help of 3D printing and femtosecond laser surface processing (Figure 9d) .[122] The spontaneous directional transport of liquids with a surface tension in the range of 15—48 mN m^{-1}, which is an inspiring manifestation of selectivity. The maximum transmission speed on the FSLLS occurs when the surface tension of the liquid is lowest, up to 265.3 mm s^{-1}. The transmission characteristic can be attributed to the unique gradient distribution of the micropit structure on the surface of FSLLS and its lipophilic properties. Inspired by the continuous cross-boundary transport of water on the surface of the Nepenthes peristome, Li et al. replicated the shape of the DLP printed mold with PVA hydrogel, then demolded to form a complementary structure of the PVA hydrogel tube, and finally a scale-shrunken capillary tube with internal microstructure is obtained through solvent exchange process.[144] "Candy cane" was fabricated which shaping internal peristome-like capillary tube with a controlled self-siphon and siphon diode behavior. Under the synergistic effect of the peristome-mimetic structure and the inner curvature of the tube, there is no need of the external energy input for the directional movement of the liquid. Another work from Liang et al. demonstrated an arrow microstructure array channel fabricated using photocuring 3D printing (Figure 9e) .[145] Due to the asymmetric shape of the arrow, the liquid is subjected to the gradient Laplace force in the direction of the arrow, and a retarding force in the opposite direction that prevents backward transportation. Numerically, the arrow microarray exhibits excellent anisotropic liquid transfer capability and relatively high transmission speed, which can reach 23 mm $^{-1}$s and the ratio of transmission length to channel width (L/R) can reach ≈40. **Table 3** demonstrated the parameters of 3D-printed anisotropic water transport structures.

4.3. Applications of 3D Printed Anisotropic Liquid Transport Interfaces

The **Figure 10** illustrated the summary of bioinspired of 3D-printed structures for anisotropic water transport. Liquid anisotropic transmission is of great significance in the fields of agricultural production, energy environment, and biomedicine. Inspired by nature, researchers have developed a variety of droplet driving methods that use wettability gradients and asymmetric structures to achieve droplets. It is driven quickly and efficiently and has played an important role in the directional collection and transportation of micro-droplets, biological detection, anti-icing, power generation, and efficient heat dissipation. However, the current research still has some shortcomings. In terms of preparation, anisotropic surfaces often need to introduce micro-nano structures, which are easily destroyed by changes in temperature, pressure, and chemical environment. How to improve the stability of anisotropic surfaces is one of the difficulties in current research. In terms of application, most of the droplets driven by anisotropic surfaces are over millimeters in size. How to drive smaller droplets, develop the application of anisotropic surfaces in micron and nanoscale fluid drive, and improve the droplet drive theory, still requires further research. Precisely controlling the driving speed and distance of the droplets and realizing the refined and intelligent driving of the droplets, are also the hotspots and difficulties of the current droplet research. In addition, the development of directional transport of droplets on asymmetric surfaces for applications in microfluidic chips, biomedicine, and energy efficient collection is an important development direction in this field in the future. In short, the anisotropic surface driven droplets have the advantages of low energy consumption, high efficiency and simple method, which is

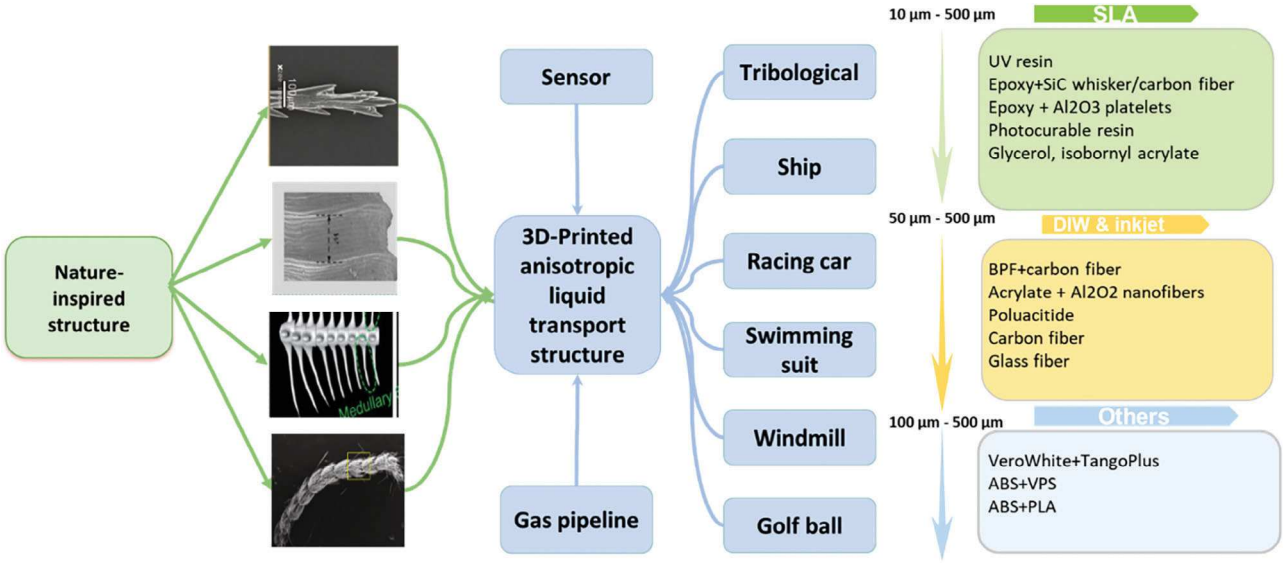

Figure 10. Summary of application of 3D-printed anisotropic liquid transport structure.

an important method commonly used in droplet manipulation. The solution to the above problems will improve the droplet driving technology and promote the development of the droplet research field to broaden the application prospects of droplet research.

5. 3D Printing of Bioinspired Interfacial Structures for Water Collection and Cleaning

5.1. Nature Inspirations for Water Collection and Cleaning

Global warming and ocean pollution have bought severe freshwater shortage problems, which negatively impacted the expected life of humans. How to proceed with water collection and oil-water separation is highly significant at this moment. Nature can bring us numerous inspirations and thoughts about the design principle of water collection structures. Some beetles in the Namib desert use fog-laden wind on their back to collect drinking water, as **Figure 11a** shows.[19] Parker et al. found that the uneven surface area can be used as a water collection surface, consisting of repeating non-waxy hydrophilic and waxy hydrophobic regions. Compared to beetles in the Namib desert, lizards (Figure 11b) can absorb water due to the unique hydrophilic honeycomb-like structure and specific geometry of capillaries.[147] Water is ingested towards the snout after accumulation in tiny capillary channels among the scales on the lizard's surface. On the other hand, spider silk (Figure 11c) is one of the most efficient water collection structures.[148,149] When placed in fog, the puffs in the spider silk shrink into periodic spindle-knots and joints. In addition to adapting to the desert's arid climate, cactus spines (Figure 11d) are used as fog collection structures by using the clusters of conical spines and belt-structured trichomes.[12] This function is based on the gradient of surface-free energy as well as the gradient of Laplace pressure. The cactus's spines structures are vital parts of recent bio-inspired 3D printing research. A bunch of studies did lots of investigating on it. The study results will be discussed in the later sections. The desert grass and bush (Figure 11e,f) surface can guide collected droplets toward the plant base to absorb sufficient water from fog in the desert.[150,151] Tiny water droplets are collected on the tips of the leaves. Once the beads become too heavy to hold, they detach into the main body section of the plant to incorporate with other fallen droplets. All those natural water-harvesting constructors bring the ideology of designing water collection structures using traditional manufacturing methods, even additive manufacturing.

5.2. Traditional Manufacturing Approach and Challenges

To achieve a bio-inspired water collection function, recent studies have been applied and gained some accomplishment by using varieties of fabrications and materials. One of the most collaborative examples is by mimicking the back surface of desert beetles, which use hydrophilic and hydrophobic regions patterns to capture fog from the air. Besides, spider silk is one of the effective tools for water collection.

Zheng et al. showed the reason for the efficient water capture of the cribellate spider is applying "wet-rebuilt" fibers.[18] Moreover, Bai et al. tested the functional fiber with periodic spindle-knots, which was inspired by spider-silk.[152] The functional fibers fabricated on a significant scale by using a fluid coating pattern can collect water in a directional method. Another study by Bai et al., is focused on the desert beetles-inspired water collecting star-shaped surfaces.[153] This surface achieved water harvesting by integrating both shape gradients and wettability. However, the traditional approach faces several issues. For instance, the materials are generally fragile and easily damaged. Besides this, the size and porous structure of materials is hard to control using traditional ways. The accuracy of the production made by the conventional approach may not reach the expected goal. To solve those problems, additive manufacturing (3D printing) has been replaced by traditional methods to overcome the existing shortcomings and bring more applications.[77]

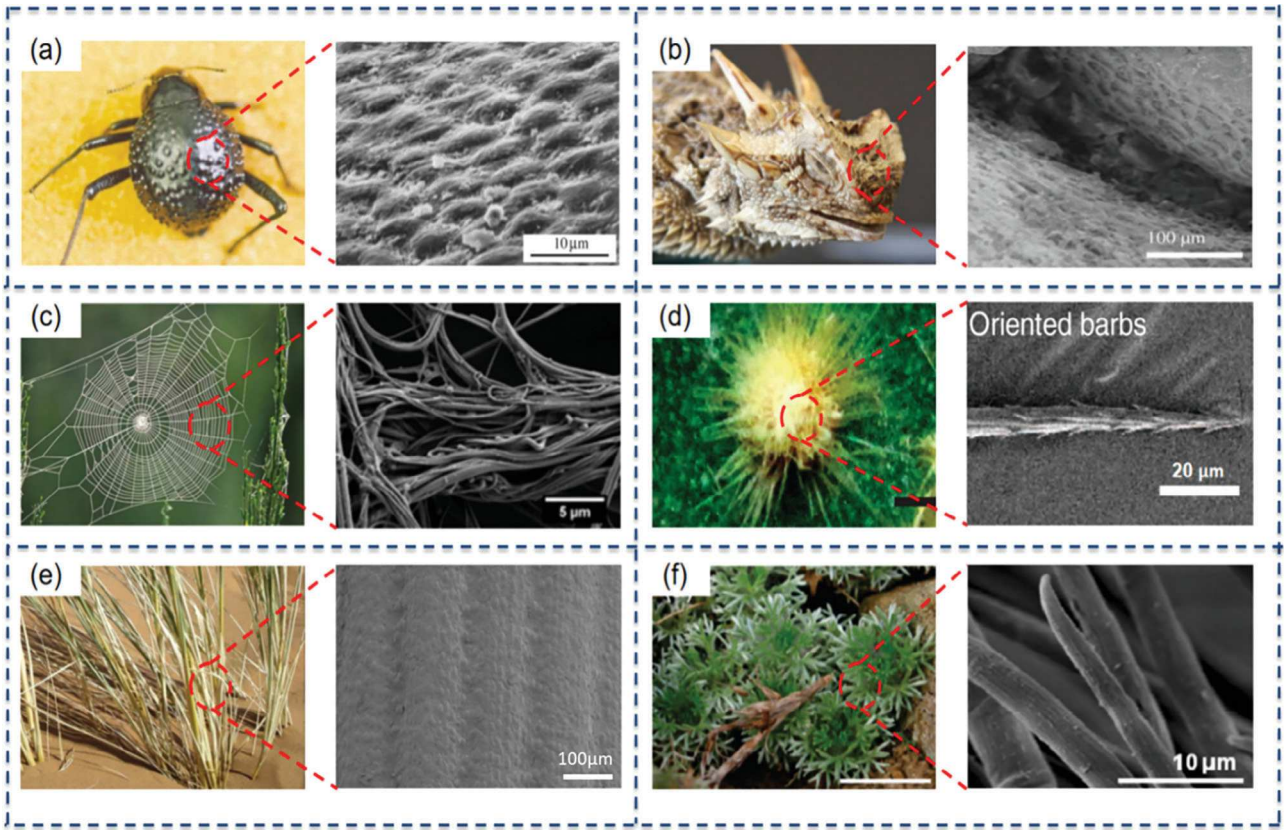

Figure 11. Bio-Inspired structures and SEM photos: a) Namib desert beetle's surface. Reproduced with permission.[19] Copyright 2001, Springer Nature. b) Lizard's surface. Reproduced with permission.[147] Copyright 2015, CC BY 4.0. c) Spider's web. Reproduced with permission.[148,149] Copyright 2018 and 2020, Elsevier and CC BY 4.0. d) Cactus' spines. Reproduced with permission.[12] Copyright 2012, Springer Nature. e) Dessert grass leaves and f) Bush leaves. Reproduced with permission.[150,151] Copyright 2012 and 2011, The Royal Society Publishing and ACS Publications.

5.3. 3D Printing of Bioinspired Structures for Water Collection and Oil-Water Separation

5.3.1. 3D Printing of Bioinspired Structures for Water Collection

As a plant living in the desert, the cactus has a water collection system based on the evenly distributed clusters of spines and trichomes on the cactus stem. By combining the mechanical perforating and template replica method, polydimethylsiloxane(PDMS) cone arrays were fabricated (**Figure 12f**) .[154] The mechanism called the inherent fog collection used by the cactus inspired the environment-friendly water collection system. The immersed surface accumulation-based 3D printing was used to approach the artificial cactus structure to make up for the low water collection efficiency defect in traditional manufacture (Figure 12a) .[37] This study illustrated that the moisture airstream around 3D printed cacti spines was improved by the hexagonally arranged clusters. The researchers compared the water weight gain of different tip angles of 3D-printed spines, resulting in 10° tip angle with a hydrophobic coating that could reach the highest weight gain of 2 mg min^{-1} mm^{-3}. In addition to the need to meet the high efficiency of waterdrop capturing, fast transport of fog drops is also necessary for 3D-printed devices. Xiao et al. inspired by the unique hierarchical structure of wheat awn designed a 3D printed artificial awn-like hierarchical structure (Figure 12b) .[146] The hierarchical structure is composed of three parts which are gradient microgrooves, conical spines, and oriented thorns. Those parts enabled the waterdrop to transform from dropwise mode to film wise mode. Compared to other individual bioinspired systems, the collection efficiency of these systems is 5.90 g/(cm^2 h), which is higher than others. Another cactus-inspired hybrid fog collection featuring longitudinal ridges on the surfaces and peristome-inspired bottom channels was developed by Liu et al. (Figure 12d) .[155] The result showed that four longitudinal ridges 3D printed spins behaved the highest water collection rate. The bottom channel with C-IAPGs played a crucial role in the route of fog translation towards the reservoir. It is difficult for a single cactus structure to achieve higher water collection efficiency on the bioinspired cactus spines' basis, the array incorporating cactus-like cone and beetle-like hydrophobic-hydrophilic character was fabricated (Figure 12c) .[156] The method is characterized by UV-induced controllable diffusion, which can break away from the photomask to regulate the hybrid wettability. The 3D printing approach can easily control the hybrid wettability of the sample surface and cone distance to optimize the water collection rate (WCR). In nature, the Sarracenia trichome with hierarchical microchannels is one of the significant water collection and transport methods. Wang et al. presented a configuration of artificial spins with barbs and hierarchical channels (SBHC) (Figure 12e).[157]

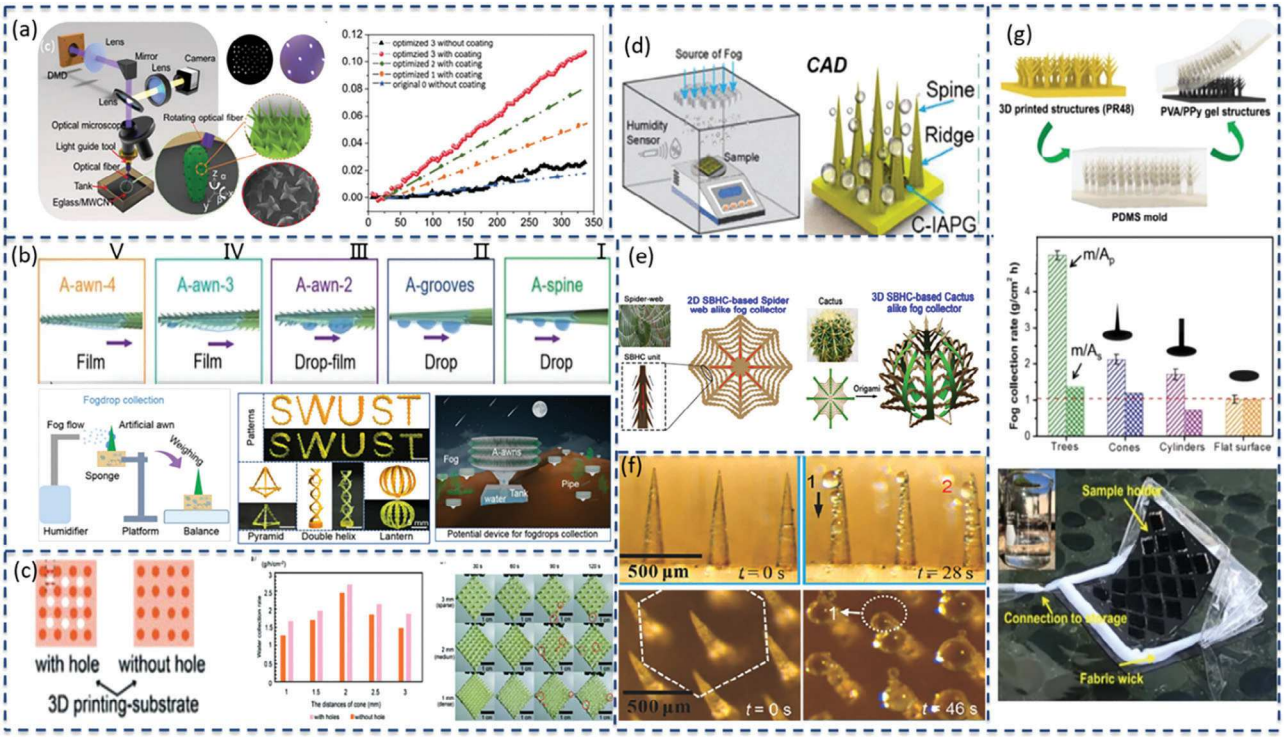

Figure 12. 3D printed bio-inspired structures for water collection: a) Sketch diagram of the ISA-based 3D printed process, and the collected water masses for different coating statues of multibranched spines over time. Reproduced with permission.[37] Copyright 2020, Wiley-VCH. b) Schematic diagrams of the fogdrop transporting process of A-spine and A-grooves systems, and comparative diagrams of the transport distances, velocities, and volumes of different artificial systems. Reproduced with permission.[146] Copyright 2020, Elsevier. c) Bioinspired cone arrays with superhydrophobic-superhydrophilic character, and cone structure with or without holes water collection rate without coating. Reproduced with permission.[156] Copyright 2021, Royal Society of Chemistry (CC BY 4.0). d) Schematic diagram of the experimental setup, and CAD model of bioinspired fog-collection structure. Reproduced with permission.[155] Copyright 2021, ACS Publications. e)Design illustration of a 2D SBHC-based spider-web-like forg collector and 3D SBHC-based cactus lie fog collector. Reproduced with permission. [157] Copyright 2020, ACS Publications. f) Comparison of the mass of the water collected on four types of surfaces along the deposition time under the same fog condition. Reproduced with permission. [154] Copyright 2014, Wiley-VCH. g) Schematic diagram of the fabrication of microstructured PVA/PPy gel membrane, and fog collection rates of different gel membranes at steady states normalized by the projected area. Reproduced with permission.[158] Copyright 2021, CC BY 4.0.

Compared with other three channels including spines with hierarchical channels (SHCs), spines with barbs and grooves channels (SBG), and spines with barb channels (SB), SBHC demonstrated the highest efficient fog harvesting. Furthermore, the researcher fabricated the bioinspired 2D spider-web fog collector and the artificial 3D cactus fog collector based on the SBHC unit. The latest research has developed a hydrogel membrane that contains a hierarchical 3D microstructure with a large surface area with both solar steam water purification function and fog collection system in an all-day freshwater harvesting system (figure 12g) .[158] In this section, 3D printing technologies based on the bioinspired structures to generate high-efficiency fog collection systems are also discussed. **Table 4** demonstrates the properties of 3D-printed water collection structures.

Table 4. A comparison of the 3D-printed bioinspired interfacial structures for water collection and cleaning.

Material	3D Printing Method	Resolution	Bioinspired effect	Properties	Application	Reference
E-glass with MWCNTs	ISA-3DP	8 μm—35 μm	Hydrophobic	The highest weight gain of 2 mg min^{-1} mm^{-3}	Potentially relieving the water crisis	[159]
Commercial hydrophilic adhesive	DLP-3DP	500 μm	Hydrophobic–Hydrophilic	Water collection rate can reach 2.46 g h^{-1} cm^{-2}	Potentially bionic fog collector	[156]
1,6-hexanediol diacrylate	Micro-Continuous Liquid Interface Printing	500 μm	Hydrophobic	Average fog-collection rate can reach 1.1×10^{-4} g min^{-1} mm^{-2}	Potentially smog removal	[155]
PVA/PPy gels	Stereolithography	30 μm	Hydrophilic	Fog collection rate (m/Ap) of ≈5.0 g cm^{-2} h^{-1}	All-day fresh water harvesting device	[160]

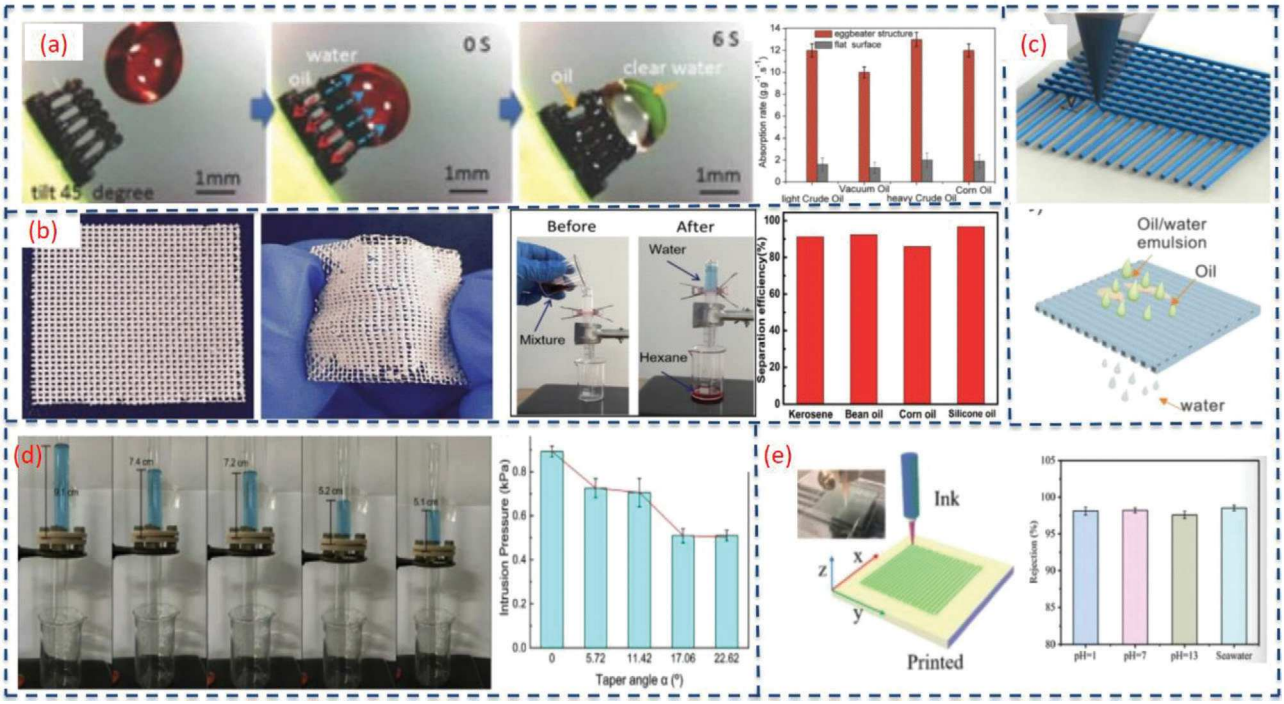

Figure 13. 3D printed structure with a) Oil/water mixture separation by the printed eggbeater structure. Reproduced with permission.[49] Copyright 2018, Wiley-VCH. b) The mesh with the superhydrophobic coating before and after bending, and oil–water separation device and process photo. Reproduced with permission.[161] Copyright 2017, Royal Society of Chemistry. c) Schematic diagram of the fused deposition modeling 3D printing process. Reproduced with permission.[162] Copyright 2019, CC BY 4.0. d) The configuration used for the separation of heavy oil/water and light oil/water mixtures, and water intrusion pressure as a function of taper angle. Reproduced with permission.[163] Copyright 2021, Elsevier. e) The printed process of the 3D printed composite membrane. Reproduced with permission.[164] Copyright 2020, Elsevier.

5.3.2. 3D Printing of Bioinspired Structures for Oil-Water Separation

Marine pollution is also an environmental issue worthy of attention in recent years. Biomimetic functional surfaces with hydrophobic properties can work on the oil-water separation issues. Yang et al. fabricated the superhydrophobic micro-scale artificial hairs with eggbeater heads inspired by *Salvinia molesta*-typed leaf (**Figure 13a**).[49] The 3D-printed eggbeater surface illustrated that even if the material has hydrophilic property, the exterior with proper micro-structured features can also show the hydrophobic property. The results showed that the different numbers of eggbeater arms could control adhesive force (from 23 μN to 55 μN) for further potential applications. Inspired by the oil absorption ability of *Molesta*-typed leaf, the 3D-printed eggbeater structure was presented as an efficient way for water-oil separation. The separation methodology uses the difference in capillary forces acting on the two phases, showing high separation efficiency. Instead of bio-inspired water-repellent structures, superhydrophobic porous membranes are the promising fabric for water-oil separation. The superhydrophobic membranes with an ordered porous structure were approached by 3D printing technology using hydrophobic nano-silica-filled polydimethylsiloxane (PDMS) ink for water-oil separation (Figure 13b) .[161] To ensure the structure won't collapse during the 3D printing process, the addition of nano-silica was added to the ink to improve the mechanical strength. By changing the roughness at the submillimeter scale, a 3D-printed superhydrophobic PDMS membrane was fabricated. Another study obtained superhydrophilic and underwater superoleophobic mesh (S-USM) with hydrogel coating via the fused deposition modeling (FDM) 3D printing by using Fe/polylactic acid (PLA) composites (Figure 13c) .[162] To increase the efficiency of oil-in-water mixture separation, salt of aluminum chloride was incorporated within the hydrogel coating, which is for strengthening the demulsification of the oil-in-water mixture. The results showed a separation efficiency of up to 85% among various mixtures of oil-water liquid. The materials made of membranes in traditional manufacturing are not stable at high temperatures. Therefore, 3D printing technology is demonstrated to develop stable and customizable structures. Herein, a ceramic material with a gradient pore structure and superhydrophilic/superhydrophobic properties was fabricated using additive manufacturing for high efficiency and high-temperature resistance (Figure 13d) .[163] The gradient pore structure developed by 3D printing in this research can support a flux that is 40% higher than that of an analogous structure with straight pores. The high-temperature resistance performance is reflected in this research as well. Compared to the room temperature, the oil-water separation performance was maintained at 97.4% of 200 °C, almost reducing a small part. In another study, the direct inkjet writing (DIW) 3D printing technology is used to manufacture a superhydrophilic and underwater superhydrophobic membrane with an ordered porous structure (Figure 13e) .[164] The result demonstrates the superhydrophilic property with contact angels in-air at about 18.14 ± 2.61°, and the

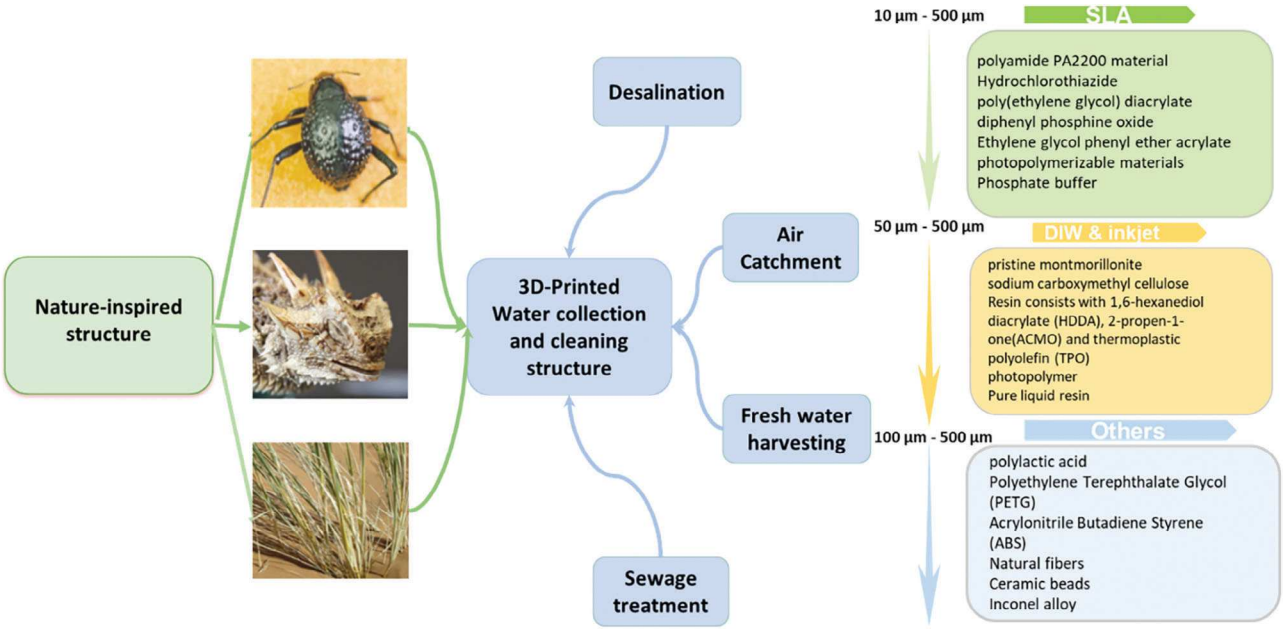

Figure 14. Summary of application of 3D-printed water collection and cleaning structure.

superhydrophobic property with a high underwater oil contact angle of ≈159.14 ± 0.59°. The optimal printed membrane maintained high oil/water separation efficiency of ≈99.0%. Compared to the traditional approach, the 3D printed membrane in this work exhibited superior mechanical stability even after 100 bending cycles, which increased the membrane service life.

5.4. Summary of Water Collection/Cleaning Applications

3D-printed bioinspired materials, processes, and applications are summarized and shown in **Figure 14**. For 3D-printed water collection and water-oil separation structures, the challenges lie in process optimization and adaptability issues.[165] Different materials and methods cause significant results in the 3D-printed structures. Herein, there is a strong need to optimize the materials and fabrication methods for the technology that requires the high efficiency and best cost-performance for the water collection water-oil separation applications.[166] In addition, potential applications of water collection structures including efficient wastewater treatment, freshwater harvesting, and air fog catchment are needed to be studied in the future.[167]

6. 3D printing of Bioinspired Interfacial Structures for Drug Delivery

6.1. Nature Inspiration for Drug Delivery

The impact of drug delivery is undeniably significant, with the potential to revolutionize the field of healthcare by offering painless and controlled methods of administering therapeutic agents. This section places a strong emphasis on the critical role that interfacial structures play in microneedles, a key enabler in enhancing the efficacy of drug delivery. Interfacial structures are intricately linked to the success of microneedles in several ways. First and foremost, they are fundamental in the reduction of insertion forces, making the process of microneedle penetration into the skin or target surface minimally invasive and virtually painless. Additionally, interfacial structures are designed to ensure secure attachment, preventing microneedles from dislodging prematurely and thereby guaranteeing that the drug or therapeutic agent is delivered precisely to the intended location. Through these enhancements, the interplay between the intricately designed structures of microneedles and their interaction with the interface contributes to the efficient and reliable delivery of drugs or biologics. Building on the foundation of enhanced drug delivery facilitated by interfacial structures, one of the most promising and innovative technologies in this domain is the utilization of microneedles. Microneedles represent a groundbreaking approach to drug delivery, with their microscopic dimensions and precisely engineered structures allowing for minimally invasive and targeted administration of therapeutic agents. By further exploring the intricate world of microneedles, we can appreciate the transformative potential of these tiny structures in the realm of healthcare and medical technology. In the following section, we delve into the introduction of microneedles, their design, functionality, and the diverse applications they offer in revolutionizing drug delivery and other areas. As they are used to pierce only the outermost layer of skin, the Microneedles (MNs) used in transdermal drug delivery typically range in size from 150 to 1500 μm in length, and 50 to 250 μm in diameter.[168–170] MNs are manufactured as patches, where tens to hundreds of MNs are placed in arrays.[171,172] The small size makes the microneedles used in transdermal drug delivery considered to be painless in comparison with traditional hypodermic needles as they only reach from 5% to 35% of the pain of a hypodermic needle.[173] Another advantage of MNs is that no requirement of the specialized training for the use.[174,175] MNs can be simply applied by pressing the patch into the targeted location. MNs, at their

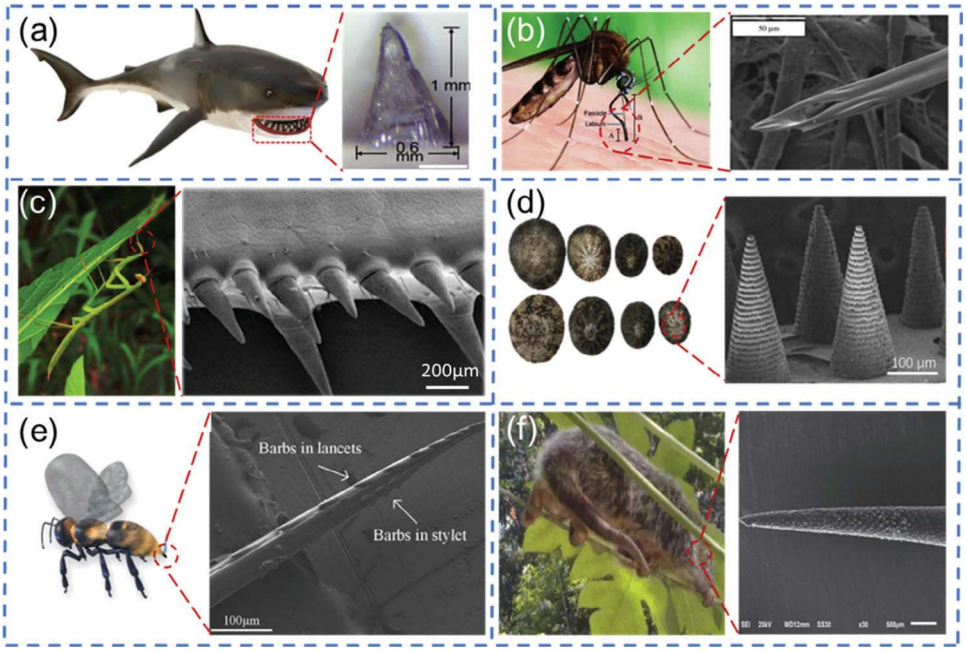

Figure 15. a) Image of shark and its tooth. Reproduced with permission. ,[179] Copyright 2021, ACS Publications. b) Image of the mosquito and SEM image of the Fascicle tip. Reproduced with permission.[13,180] Copyright 2008 and 2018, IOP Publishing and CC BY 4.0. c) Image of a Praying mantis and SEM image of the spikes on the Mantis' forearm. Reproduced with permission.[181] Copyright 2019, Elsevier. d) Image of a Limpet with SEM image of the limpet's teeth. Reproduced with permission.[182] Copyright 2021, Wiley-VCH. e) Image of a honeybee with SEM image of a Honeybee stinger. Reproduced with permission.[183,184] Copyright 2017 and 2022, Elsevier. f) Image of a Porcupine and SEM image of its Quills. Reproduced with permission.[185] Copyright 2016, CC BY 4.0.

inception, began as very simple shapes consisting of cones and pyramids.[176] While the disadvantages of these simple shapes are that small size microneedles are susceptible to fracture and bending during insertion. Due to the increase in manufacturing technologies capable of producing more complex microstructures, the possibility of creating geometrically complex MNs with advanced capability has also grown.[177,178] As the capability to manufacture more complex microstructures has been improved, designers have taken inspiration from many natural microstructures in the creation of novel MN designs with enhanced features. For example, a shark tooth-inspired microneedle is shown in **Figure 15**a.[179] Microneedles can utilize stable adhesion to the skin when applied as a patch. Mosquitos utilize a Fascicle tip with a hollow proboscis to extract blood through the skin at the same size scale as MNs, as shown in Figure 15b.[13,180] Microneedles designed after the mosquito proboscis can achieve enhanced drug delivery when combined with microfluidic devices. Praying Mantis uses an array of sharp tips between their forearms to trap prey in Figure 15c.[181] A microneedle array designed after the forearms of the praying mantis would achieve higher adhesion to the skin. Limpets have developed incredibly strong teeth that have a similar size to MNs, as shown in Figure 15d.[182] Microneedles designed after limpet teeth could achieve a higher strength to avoid fracture.[22] Besides, honeybees have developed stingers with barbs attached that make them harder to remove, as shown in Figure 15e.[183,184] Microneedles designed after the honeybee stinger barbs could achieve a higher pull-out force than a microneedle without the barbs. Finally, porcupines have quills with microscale barbs that they use for defense against predators, as shown in Figure 15f.[185] A microneedle designed after the porcupine quill barbs would also achieve a higher pull-out force. Microneedles have gained prominence for their applications in drug delivery, diagnostics, and tissue sampling. These applications inherently involve the interaction of microneedles with biological surfaces, highlighting the critical role of surface and interfacial science. The design and properties of microneedles, including their sharpness, material composition, and how they interact with biological fluids, are key aspects of their functionality.

6.2. Traditional Manufacturing Approach and Challenges

As it stated previously, the first MNs were manufactured using the simple cone and pyramidal shapes, which was mainly accomplished through milling and etching, one of the most advanced manufacturing techniques available at the time. While it is possible to create more advanced microscale features through these means. Other manufacturing methods currently allow a higher degree of complexity in such features. Additive manufacturing (also known as 3D printing) is particularly well suited to the creation of highly complex shapes due to its layer-by-layer build process. The ability to manufacture highly complex microstructures with additive manufacturing has increased tremendously in the past few decades, due to the increase in the number of devices capable of manufacturing on the micro and nanoscale level. The resolution and printing size of these additive manufacturing techniques continue to improve allowing for the creation of even more complex microscale structures as time goes on. An increase

in the manufacturing speed along with new materials and methods makes the use of additive manufacturing techniques more attractive in the creation of novel biomimetic microneedle designs.

6.3. 3D Printing of Bioinspired Structures for Drug Delivery

6.3.1. Interfacial Structures Design of Microneedle for Properties Enhancement

Microneedles, especially 3D printed ones, have fine, precisely designed structures with micrometer-scale dimensions. They are engineered to gently and precisely penetrate the skin or target surface. 3D printing technology allows for precise control of the microneedle's shape and size. The interaction with the skin is designed to create minimally invasive, micrometer-scale punctures. These micropores are typically smaller than traditional hypodermic needle punctures, which significantly reduces discomfort and tissue damage. In Luzuriaga et. al. study,[186] the researchers have introduced a novel approach to microneedle array fabrication by employing fused deposition modeling (FDM) 3D printing with biodegradable polylactic acid (PLA). The research demonstrates the feasibility of these microneedles, highlighting their potential in painless and sanitary transdermal drug delivery, with the added benefit of controlled drug release through the natural degradability of PLA within the skin. Surface modifications are pivotal in enhancing the capabilities of 3D printed microneedles. These modifications can include coatings, bioactive compounds, or specific material choices that optimize drug delivery, skin adhesion, and other functionalities. In Economidou et. al. study,[187] 3D printed microneedle arrays were manufactured via stereolithography (SLA) using biocompatible resin for transdermal insulin delivery. Micro-CT analysis confirmed strong adhesion of the insulin-coated films, even after skin penetration, and in vivo animal trials demonstrated rapid insulin action, effective hypoglycemia control, and stable plasma glucose levels over a 4-hour period, highlighting the promising potential of this technology for improved insulin delivery and glucose management. The design of biomimetic microneedles can take on many shapes and forms (**Figure 16a**) .[21] Zhang et al. took inspiration from the suckers present on the tentacles of octopus to create a microneedle array with enhanced adhesion as shown in Figure 16b.[188] These microneedles utilize a hierarchical structure of a hydrogel microneedle tip and polydopamine base loaded with polymyxin to increase the antibacterial properties of the microneedle. Each microneedle tip is surrounded by six suctions cup-shaped concave cavities. These suction cups provide the microneedle array with enhanced adhesion. The suction cup microneedle array has a peeling adhesion of 1.5 N cm^{-2} when dry and a peeling adhesion of 1.25 N cm^{-2} in comparison with a microneedle array without the suction cups achieving a peeling adhesion of 0.6 N cm^{-2} dry and 0.3 N cm^{-2} wet.

Han et al. designed a backwards-facing barbed microneedle inspired by the barbs found in honeybee stingers and porcupine quills as shown in Figure 16c.[189] These backward-facing barbs increase the force needed to pull the microneedle array out of the tissue as the backwards-facing barbs lock into the tissue after penetration. This is advantageous for microneedles as it increases the ability of the microneedle array to achieve long-term controlled biosensing or drug delivery by reducing the likelihood of the microneedle array being removed during regular activity. In this study, the barbed microneedle increased the force needed for pull-out from 0.05 N for the barbless microneedle to 0.175 N for the barbed microneedle array. An increase of roughly 5 times the force over the barbless microneedle. Amer et al. who also inspired by the barbs on natural structures have created a swellable microneedle with an interlocking feature in the middle of the microneedle as shown in Figure 16d.[190] This microneedle is created out of a material that takes in moisture after insertion. This absorption of liquid causes the microneedle to swell and grow larger which includes the interlocking feature in the middle of the microneedle. Due to this expansion in size this microneedle experiences an enhancement in adhesion with the tissue. Plamadeala et al. were inspired by the scent efferent systems of some European true bugs to create a microneedle with directional liquid transport as shown in Figure 16e.[191] The beetles use microstructures on their bodies to unidirectionally transport defensive liquids from where they are secreted to the locations as the liquid evaporates. By mimicking these microstructures on the surface of a pyramidal microneedle, a unidirectional transport of a liquid coating of vaccine or drugs can be achieved on the microneedle to rapidly coat the microneedle. Microneedles with hollow tips also mimic the microstructure of mosquito proboscis. As shown in Figure 16f. Yadav et al. created a hollow microneedle that utilizes a sharp tip with a side opening followed by a hollow tube that is similar to a mosquito proboscis.[192] This enables the microneedle to be used for the more constant application of liquid drugs through a microfluidic pump. This is an improvement over many coated microneedle designs which only allow for a limited application of any drug or vaccine before they would need to be recoated and replaced. Zhang et al. developed a technique utilizing ferrofluid to create a mold mimicking the forearms of the Praying mantis illustrated in Figure 16g.[181] These angled microneedles increased the adhesion of the microneedle patch. In testing the load-bearing capability of the patch when placed at a 180-degree angle to the skin increased from 1 g with a patch consisting of MNs at a 90-degree angle to the patch to 3 g with a patch consisting of MNs at a 30-degree angle to the patch. Demonstrating the enhanced adhesion, the clasping design brings. In Figure 16h, inspired by the strength observed in Limpet teeth Li et al. fabricated microneedles which contained aligned Iron Oxide bundles.[193] These bundles of Iron Oxide created a microneedle with greater compressive strength. With a concentration of 2.5% Iron Oxide the microneedles reached their greatest compressive modulus of 2500 MPa which was almost 5 times higher than the polymer microneedle reached without the aligned Iron Oxide. **Table 5** compares the properties of 3D-printed biomimetic microneedle structures.

6.3.2. Current 3D Printing Methods for Microneedles Fabrication

To manufacture biomimetic microneedles, a variety of additive manufacturing techniques are employed. Most of these techniques employ stereolithography in some fashion due to the enhanced resolution and structural freedom it allows in the fabrication process. **Figure 17a** represents a typical stereolithography printing process used in the fabrication of

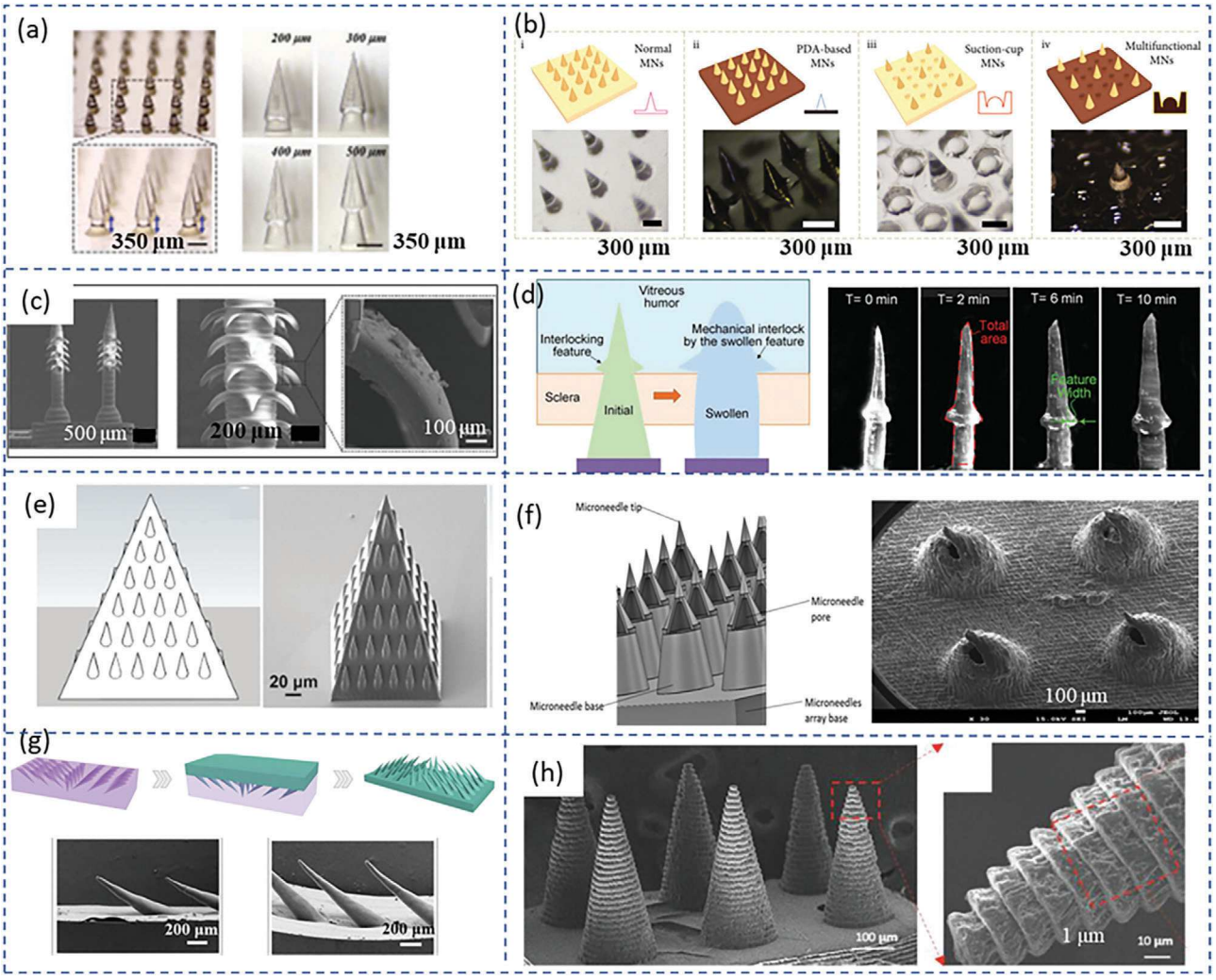

Figure 16. a) Images of stacked pagoda microneedles created through molds. Reproduced with permission.[21] Copyright 2021, Elsevier. b) CAD and Microscopic images of the octopus inspired microneedles. Reproduced with permission.[188] Copyright 2020, CC BY 4.0. c) SEM images of the barbed microneedles created through 4D printing. Reproduced with permission.[189] Copyright 2020, Wiley-VCH. d) Illustration of the concept of the interlocking feature and photos of swelling of MN at 0, 2, 6, and 10 min. Reproduced with permission.[190] Copyright 2020, Wiley-VCH. e) CAD model of the structured MN and the non-structured MN. Reproduced with permission.[191] Copyright 2020, Springer Nature. f) CAD model and FESEM image of the 3D-printed HMNs array top view. Reproduced with permission.[192] Copyright 2021, Elsevier. g) Schematic illustration of serrated clamping MN arrays fabrication process and SEM images of MNs with different inclination angles. Reproduced with permission.[181] Copyright 2019, Elsevier. h) SEM images of MF-3D-printed MN array. Reproduced with permission.[193] Copyright 2021, Wiley-VCH.

microneedles. Namely, that a build plate is lowered into a photosensitive resin. That resin is then exposed to Ultraviolet light in a desired shape which polymerizes the resin and solidifies it to the build plate. The build plate then moves upward, and the next layer is exposed as the process repeats until the finished part is completed.[187,197–200] Another fabrication method for biomimetic microneedles is through the use of magnetorheological lithography drawing as shown in Figure 17b. This novel method was developed by Chen et al. and utilizes a magnetic field to assist in the creation of micro barbs along the surface of a microneedle.[201] Initially, a microneedle is fabricated, following this, a curable magnetorheological fluid is applied in droplets along the outside of the microneedle and drawn perpendicularly outward to create the micro barbs. With an external magnetic field, the angle of these barbs is altered such that the tips of the micro barbs face closer to the base of the microneedle. Another method of fabricating biomimetic microneedles is by using negative molds as presented in Figure 17c. Many such molds will be created through the initial use of an additively manufactured master.[202–204] A curable resin is then introduced into this mold and cured through UV light to fabricate a microneedle. A study by Zhang et al. goes one step further by adding a heightening pad and reinserting the fabricated microneedle into the mold to repeat the process.[21] Through this means, a microneedle is fabricated with several conic structures stacked on top of each other which mimics the effects of barbs. Li et al. utilized a magnetic field to assist in the printing of microneedles with enhanced compression resistance and a high mechanical integrity as shown

Table 5. A comparison of the 3D-printed bioinspired interfacial structures for drug delivery.

Material	3D Printing Method	Resolution	Bioinspired effect	Properties	Application	Reference
Nextdent Ortho Rigid resin	stereolithography	1000 µm	Hydrophilic	Maximum compression forces up to 400 N	Curved HMN suitability for on-body applications.	[194]
Polymeric materials mixed with an active agent	Two-photon polymerization (TPP) lithography	5 µm	Hydrophilic	Impact energy of 0.4 ± 0.01 J cm^{-2}	Potential transdermal drug	[195]
Biocompatible Class I resin	Stereolithography	950 µm	Efficient penetration	The fracture force was ≈12 N at 0.101 mm	Transdermal delivery of high molecular weight antibiotics	[196]
Carbonyl iron micro particles mixed with the Eglass resin	Magnetic fields-3DP	10 µm	Mechanically reinforced	Pierce the PDMS with a force of 0.35 N	Potential biomedical and clinical	[182]

in Figure 17d.[193] Their study utilized a magnetic field to align Iron Oxide bundles within a polymer to mimic the structure of limpet teeth. Direct Laser Writing (DLW) and Two-Photon Direct Laser Writing (TP-DLW) are another two prominent methods of fabricating biomimetic microneedles.[205–207] In DLW, a laser is used to draw a pattern and cure a photoresist resin onto a build plate. The build plate is then moved, and the next layer of the object is drawn and cured onto the part. TP-DLW utilizes femtosecond pulsed lasers to cure the resin in a very localized region and thus achieve a resolution in the nanoscale range. An example of the process for these fabrication methods is presented in Figure 17e.[208] The fabrication of biomimetic microneedles can also include 4D printing. The fourth dimension in the printing process is a preprogrammed shape change of the object with the introduction of environmental stimuli. Han et al. presented a method of utilizing the natural tendency of photopolymerization to create a gradient of crosslinking monomers within each layer of the part to induce deformation and create backwards facing barbs shown in Figure 17f.[189] During the photopolymerization process crosslinking of the monomers occurs with a higher density at the surface closest to the source of light and the bottom of the layer contains more unlinked monomers. It means that with a wash in ethanol the unlinked monomers at the bottom of the cured layer can dissolve from the part. This creates a situation where the bottom surface has open spaces due to the dissolved unlinked monomers and during the drying process that bottom surface shrinks and the layer bends downward.

6.4. Summary of Interfacial Structured for Drug Delivery

To date, there have been many achievements in the advancement of microneedles for applications such as transdermal delivery of drugs in the medical field. There has been an increase to multiple means of production through different types of stereolithography as discussed above. The advancements in design through continued research and increased additive manufacturing capabilities include increased complexity of structures. This higher complexity allows for increased efficiency and capabilities in microneedle uses including increases in; speed/efficiency of drug delivery, consistency of drug/vaccine application, adhesion/retraction, and compressive strength. Although great advances have been made in the design, production, and utilization of microneedles, there are challenges to be overcome in future research, such as limited resolution and durability of materials available via different additive manufacturing processes, the ability to scale up or mass produce additively manufactured MNs, and the ability to distribute MNs produced by additive manufacturing means in terms of durability and transportability. Many materials used in stereolithography, and related types of 3D printing are heat sensitive, and the structures are produced on such a microscopic scale as to be somewhat fragile, even with advances in structural integrity as mentioned above. These could be potential hurdles to shipping and storage of such products leading to an increase in cost that would be less efficient. Also is the production time/scale; due to the current size limits of additive manufacturing machinery, a machine can only produce a limited amount of product at any given time. Compared to more traditional manufacturing techniques these amounts can be quite small with a limited time: quantity ratio. Biomimetic microneedles have the potential to be applied in a variety of areas and the enhanced properties demonstrated make them an attractive option over traditional microneedles. Due to their small size and unique surface properties, microneedles are engineered to interact with biological surfaces, such as the skin. The sharp tips and surface coatings play a crucial role in minimizing discomfort and tissue damage during insertion. Surface engineering techniques, including surface modifications and coatings, are employed to optimize the interaction between microneedles and biological interfaces, enhancing their performance and patient comfort. Some areas of application are in transdermal drug delivery, ocular drug delivery, vaccine delivery, hemostasis, and glucose detection (**Figure 18**).

7. Conclusion

In this review, several 3D printed bio-inspired surface structure was demonstrated in aspect of the applied materials, functional designs, and various applications. Based on the applications, the design of the 3D-printed structures can be categorized as superhydrophobic structures, structures for drag force reduction,

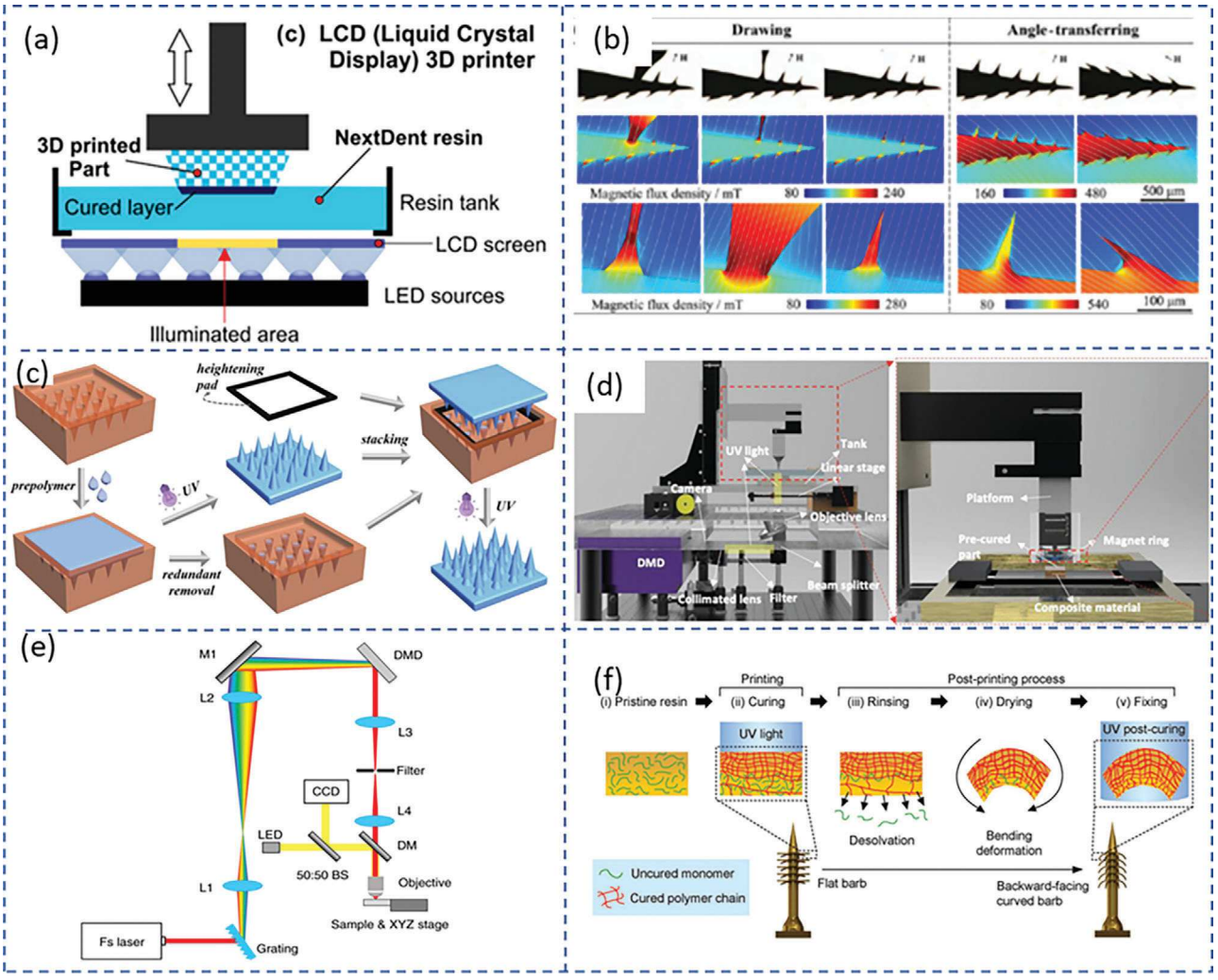

Figure 17. a) A diagram of the printing process used for LCD 3D printers. Reproduced with permission.[194] Copyright 2021, Elsevier. b) Images and magnetic flux density images of the printing process used to create barbed microneedles through Magnetorheological lithography. Reproduced with permission.[201] Copyright 2018, ACS Publications. c) Diagram of the process used to create barbed microneedles through molds. Reproduced with permission.[21] Copyright 2021, Elsevier. d) Diagram of the platform set up used to create a magnetic field-assisted 3D printing process. Reproduced with permission.[193] Copyright 2021, Wiley-VCH. e) Images of the printing process used for Direct Laser Writing. Reproduced with permission.[208] Copyright 2019, CC BY 4.0. f) Images of the 4D printing process used by Han et al. to create barbed microneedles. Reproduced with permission.[189] Copyright 2020, Wiley-VCH.

microscale surface structures with anisotropic water transport, surfaces for water collection and oil/water separation, and microneedle structures. The optimized designs of the 3D-printed bioinspired surface structures will have a promising potential as the next generation of multi-functional materials with low-cost, high efficiency, and excellent performance. With the fast development of 3D printing technology, we expect that 3D-printed surface/interface structures will solve the following challenges:

First, the materials for microscale 3d printing are still limited to be polymer-based resins, the metal and ceramic based 3d printing methods have the limited capability for fabricating nanoscale and microscale structures. This prohibits the potential applications for functional microscale structures, for example, the polymeric based materials cannot be used for the application of superhydrophobic structures in harsh environments such as high temperature. Therefore, new types of materials for harsh environments or the high-resolution printing process for metals/ceramics/composites need to be developed. The microneedle patch for drug delivery presents yet another instance where the current state-of-the-art is constrained by the limited availability of materials, specifically polymeric resins. Moreover, the mechanical properties of these materials are suboptimal, and as such, new biocompatible and/or biodegradable materials such as polymers, composites, among others, must be developed for the controllable release of drugs for the potential applications in biomedical engineering. Furthermore, novel 3d printing technology needs to be developed for the fabrication of composites with controllable aligned fillers to further improve the mechanical properties, which is widely found in natural structures. Also, another way may be the integration with traditional manufacturing

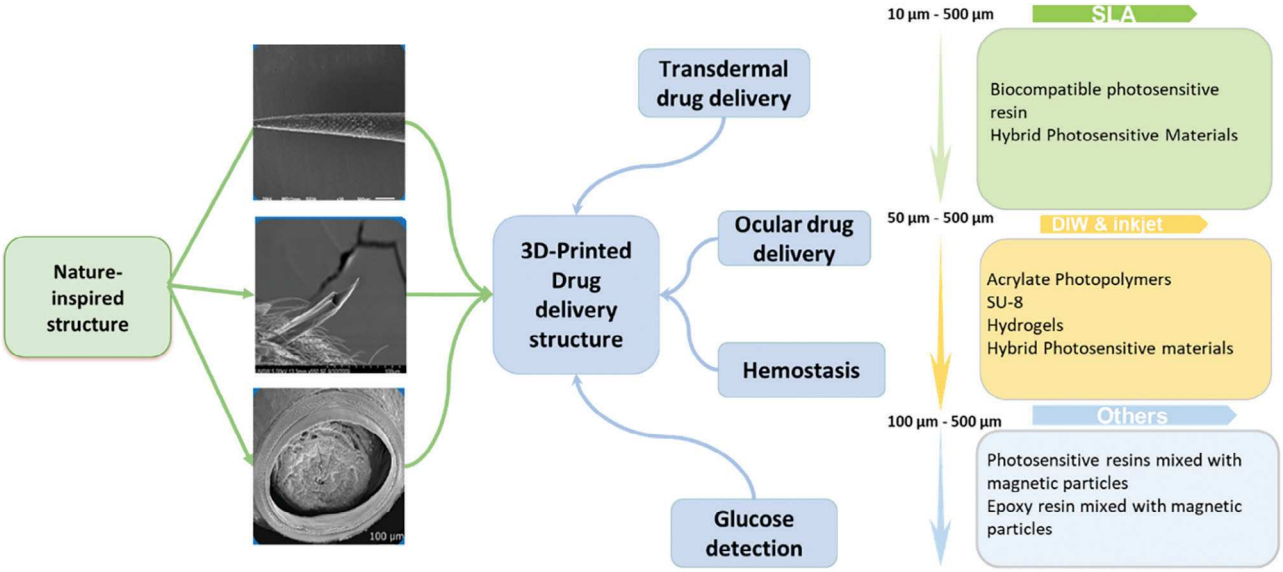

Figure 18. Summary of application of 3D-printed drug delivery structure.

technology such as sputtering or electrochemical deposition for the coating of ceramic or metal layers to improve the mechanical performance.

Second, a critical area of focus for the biomimetic design of engineering functional structures is the need to investigate natural structures' mechanisms in greater depth. While existing research has successfully identified microscale structures with functional surface/interface properties, there remain numerous natural structures whose mechanisms remain largely unexplored. By studying natural structures, researchers can gain a greater understanding of the evolution of functional structures and uncover innovative ways to apply these insights to engineering design and applications. One such example is the thermal control mechanism exhibited by silver ants in desert environments. While this mechanism has been previously documented, further work is required to investigate the protective mechanisms of these ants and explore how these insights could be applied to the design and development of radiative cooling devices for energy-efficient applications. To achieve this, optimized surface structures will be developed to facilitate multifunctional

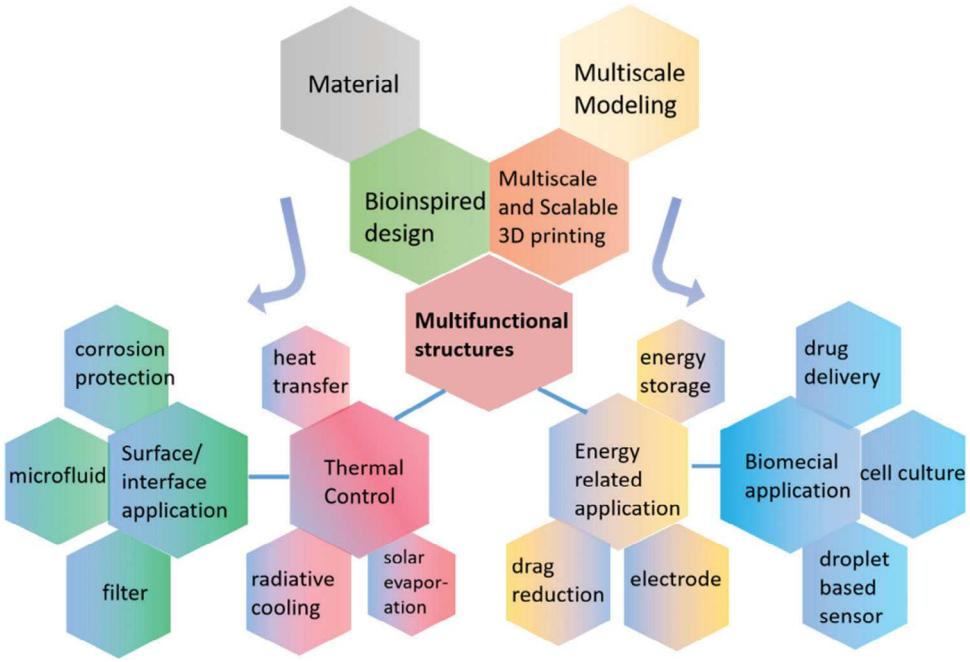

Figure 19. Perspective of the development for bioinspired 3D printing for various applications.

applications. At present, the design of surface structures is primarily inspired by single natural structures, resulting in limited functionality. Therefore, in the future, it will be crucial to combine multiple bio-inspired structures in the design of surfaces to achieve a more comprehensive range of functions. Ultimately, such efforts will contribute to the development of innovative engineering solutions that can address numerous societal challenges.

Third, the resolution of 3D printing processes for surface structures will significantly be improved to fabricate microscale or even nanoscale structures. Currently, the printed sample, such as microneedle or superhydrophobic structures, remain the resolution in micrometers level, which will influence the performance of the printed sample. Hence, optimizing the resolution of 3D printing processes for printing bio-inspired surface may be effective methods to form complex microstructure with multifunctionalities. While the TPP 3D printing method can fabricate nanoscale structures, the resolution is limited to ≈100 nm, and the total size of the structure is restricted to the microscale. Thus, there is a need to develop new processes capable of producing hierarchical structures that range in size from several nanometers to the meter scale, fully mimicking the scale and functionalities of natural structures. Integrating 3D printing with other manufacturing techniques, such as laser scanning or field-assisted alignment, as well as sputtering on microscale 3D-printed structures to generate nanoscale textures, may offer a viable solution for fabricating large area structures with nanoscale features. Moreover, the multiscale modeling of 3D printed hierarchical structures requires improvement to guide the design and fabrication of functional structures. In doing so, researchers can more effectively create bio-inspired surface structures that offer enhanced performance capabilities and contribute to addressing pressing societal needs.

Lastly, the printing time of the current 3D-printing processes will be further reduced while still retaining the superior performance. In the future, advanced bio-inspired surface structures in micro-scale with high resolution will be more widely available for customized designs and massive use in industrial areas. Therefore, it is imperative to develop new manufacturing methods that significantly reduce processing time to meet the demands of large-scale production. Recent advancements in volumetric 3D printing and continuous 3D printing methods have shown promise in addressing the limitations associated with layer-based 3D printing, while simultaneously improving fabrication efficiency. Adopting these novel manufacturing methods is essential to meet the growing demand for efficient and cost-effective production of biomimetic structures, facilitating the development of innovative technologies and solutions to address pressing bionic manufacturing needs (**Figure 19**).

Acknowledgements

Q.H., T.T., and Y.Z. contributed equally to this work. Y.Y. acknowledges funding from the National Science Foundation (no. CMMI-2113727), X. L. acknowledges funding from the National Science Foundation (no. CMMI-2114119).

Conflict of Interest

The authors declare no conflict of interest.

Keywords

3D printing, bioinspired design, functional structures, surface and interface structures

Received: August 8, 2023
Revised: November 2, 2023
Published online: December 3, 2023

[1] Y. Si, Z. Dong, L. Jiang, *ACS Cent. Sci.* **2018**, *4*, 1102.
[2] S. Das, S. Kumar, S. K. Samal, S. Mohanty, S. K. Nayak, *Ind. Eng. Chem. Res.* **2018**, *57*, 2727,
[3] Y. Wang, S. E. Naleway, B. Wang, *Bioact. Mater.* **2020**, *5*, 745.
[4] D.-D. Han, Q. Cai, Z.-D. Chen, J.-C. Li, J.-W. Mao, P. Lv, B.-R. Gao, *Front. Chem.* **2020**, *8*, 692.
[5] B. Su, Y. Tian, L. Jiang, *J. Am. Chem. Soc.* **2016**, *138*, 1727.
[6] M. Ghasemlou, F. Daver, E. P. Ivanova, B. Adhikari, *J. Mater. Chem. A* **2019**, *7*, 16643.
[7] T. Darmanin, F. Guittard, *J. Mater. Chem. A* **2014**, *2*, 16319.
[8] Q. He, Y. Zeng, L. Jiang, Z. Wang, G. Lu, H. Kang, P. Li, B. Bethers, S. Feng, L. Sun, P. Sun, C. Gong, J. Jin, Y. Hou, R. Jiang, W. Xu, E. Olevsky, Y. Yang, *Nat. Commun.* **2023**, *14*, 6477.
[9] S. Latthe, C. Terashima, K. Nakata, A. Fujishima, *Molecules* **2014**, *19*, 4256.
[10] B. Dean, B. Bhushan, *Philos. Trans. Royal Soc. A: Math., Phys. Eng. Sci.* **2010**, *368*, 4775.
[11] H. Chen, P. Zhang, L. Zhang, H. Liu, Y. Jiang, D. Zhang, Z. Han, L. Jiang, *Nature* **2016**, *532*, 85.
[12] J. Ju, H. Bai, Y. Zheng, T. Zhao, R. Fang, L. Jiang, *Nat. Commun.* **2012**, *3*, 1247.
[13] M. Ramasubramanian, O. Barham, V. Swaminathan, *Bioinspir. Biomim.* **2008**, *3*, 046001.
[14] X. Gao, L. Jiang, *Nature* **2004**, *432*, 36.
[15] S. Nishimoto, B. Bhushan, *RSC Adv.* **2013**, *3*, 671.
[16] W. Barthlott, T. Schimmel, S. Wiersch, K. Koch, M. Brede, M. Barczewski, S. Walheim, A. Weis, A. Kaltenmaier, A. Leder, H. F. Bohn, *Adv. Mater.* **2010**, *22*, 2325.
[17] H. Chen, T. Ran, Y. Gan, J. Zhou, Y. Zhang, L. Zhang, D. Zhang, L. Jiang, *Nat. Mater.* **2018**, *17*, 935.
[18] Y. Zheng, H. Bai, Z. Huang, X. Tian, F.-Q. Nie, Y. Zhao, J. Zhai, L. Jiang, *Nature* **2010**, *463*, 640.
[19] A. R. Parker, C. R. Lawrence, *Nature* **2001**, *414*, 33.
[20] G. Ma, C. Wu, *J. Control. Release* **2017**, *251*, 11.
[21] X. Zhang, G. Chen, L. Cai, Y. Wang, L. Sun, Y. Zhao, *Chem. Eng. J.* **2021**, *414*, 128905.
[22] A. H. Barber, D. Lu, N. M. Pugno, *J. R. Soc., Interface* **2015**, *12*, 20141326.
[23] G. Wen, Z. Guo, W. Liu, *Nanoscale* **2017**, *9*, 3338.
[24] Y. Yang, X. Song, X. Li, Z. Chen, C. Zhou, Q. Zhou, Y. Chen, *Adv. Mater.* **2018**, *30*, 1706539.
[25] K. Maghsoudi, E. Vazirinasab, G. Momen, R. Jafari, *Ind. Eng. Chem. Res.* **2020**, *59*, 9343.
[26] P. N. Saltuganov, A. A. Ionin, S. I. Kudryashov, A. A. Rukhadze, A. I. Gavrilov, S. V. Makarov, A. A. Rudenko, D. A. Zayarny, *J. Russian Laser Res.* **2015**, *36*, 81.
[27] K. Tsougeni, N. Vourdas, A. Tserepi, E. Gogolides, C. Cardinaud, *Langmuir* **2009**, *25*, 11748.
[28] M. Ma, Y. Mao, M. Gupta, K. K. Gleason, G. C. Rutledge, *Macromolecules* **2005**, *38*, 9742.
[29] D. Zhang, L. Li, Y. Wu, B. Zhu, H. Song, *Appl. Surf. Sci.* **2019**, *473*, 493.

[30] Y.-S. Leung, T.-H. Kwok, X. Li, Y. Yang, C. C. L. Wang, Y. Chen, *J. Comput. Info. Sci. Eng.* **2019**, *19*, 021013.
[31] X. Li, Y. Chen, *J. Manuf. Processes* **2017**, *28*, 531.
[32] X. Li, B. Xie, J. Jin, Y. Chai, Y. Chen, *Procedia. Manuf.* **2018**, *26*, 1023.
[33] X. Li, H. Mao, Y. Pan, Y. Chen, *J. Manuf. Sci. Eng.* **2019**, *141*, 081007.
[34] D. Joralmon, E. Amonoo, Y. Zhu, X. Li, *J. Manuf. Sci. Eng.* **2022**, *144*, 041012.
[35] T. Tang, B. Ahire, X. Li, *J. Manuf. Sci. Eng.* **2022**, *145*, 011004.
[36] L. Tiwari, T. Tang, J. Rong, W. Shan, Y. Yang, X. Li, *J. Mater. Sci. Technol. Res.* **2022**, *9*, 105.
[37] X. Li, Y. Yang, L. Liu, Y. Chen, M. Chu, H. Sun, W. Shan, Y. Chen, *Adv. Mater. Interfaces* **2020**, *7*, 1901752.
[38] X. Li, Y. Yang, presented at *Int. Sym. on Flexible Automation*, American Society of Mechanical Engineers, New York, **2020**, https://doi.org/10.1115/ISFA2020-9644.
[39] X. Li, Y. Yang, B. Xie, M. Chu, H. Sun, S. Hao, Y. Chen, Y. Chen, *Adv. Mater. Technol.* **2019**, *4*, 1800476.
[40] Y. Yang, X. Li, Y. Chen, in *Manufacturing In The Era Of 4th Industrial Revolution: A World Scientific Reference*, *3*, World Scientific Publishing Co., Singapore **2021**.
[41] Y. Yang, Z. Wang, Q. He, X. Li, G. Lu, L. Jiang, Y. Zeng, B. Bethers, J. Jin, S. Lin, S. Xiao, Y. Zhu, X. Wu, W. Xu, Q. Wang, Y. Chen, *Research* **2022**, https://doi.org/10.34133/2022/9840574.
[42] Y. Yang, X. Li, M. Chu, H. Sun, J. Jin, K. Yu, Q. Wang, Q. Zhou, Y. Chen, *Sci. Adv.* **2019**, *5*, eaau9490.
[43] Y. Zhu, T. Tang, S. Zhao, D. Joralmon, Z. Poit, B. Ahire, S. Keshav, A. R. Raje, J. Blair, Z. Zhang, X. Li, *Addit. Manuf.* **2022**, *52*, 102682.
[44] C. Yan, P. Jiang, X. Jia, X. Wang, *Nanoscale* **2020**, *12*, 2924.
[45] S. Hong, Y. Shi, R. Li, C. Zhang, Y. Jin, P. Wang, *ACS Appl. Mater. Interfaces* **2018**, *10*, 28517.
[46] C. Lu, X. Chen, *EcoMat* **2022**, *4*, 12181.
[47] X. Meng, Z. Cai, Y. Zhang, X. Hu, Z. Xing, Z. Huang, Z. Huang, Y. Cui, T. Hu, M. Su, X. Liao, L. Zhang, F. Wang, Y. Song, Y. Chen, *Nat. Commun.* **2020**, *11*, 3016.
[48] H. Gong, S. Luo, H. Li, S. Liu, *Mater. Technol.* **2020**, *37*, 1989.
[49] Y. Yang, X. Li, X. Zheng, Z. Chen, Q. Zhou, Y. Chen, *Adv. Mater.* **2018**, *30*, 1704912.
[50] C.-K. Nien, H. H. Yu, *Mater. Chem. Phys.* **2019**, *227*, 191.
[51] Z. Cheng, H. Han, F. Wang, Y. Yan, X. Shi, H. Liang, X. Zhang, Y. Shuai, *Nano Energy* **2021**, *89*, 106377.
[52] H.-J. Yoon, D.-H. Kim, W. Seung, U. Khan, T. Y. Kim, T. Kim, S.-W. Kim, *Nano Energy* **2019**, *63*, 103857.
[53] D. Mandt, P. Gruber, M. Markovic, M. Tromayer, M. Rothbauer, S. R. A. Kratz, S. F. Ali, J. V. Hoorick, W. Holnthoner, S. Mühleder, P. Dubruel, S. V. Vlierberghe, P. Ertl, R. Liska, A. Ovsianikov, *Int. J. Bioprint.* **2018**, *4*, 144.
[54] Y. Yang, Z. Chen, X. Song, Z. Zhang, J. Zhang, K. K. Shung, Q. Zhou, Y. Chen, *Adv. Mater.* **2017**, *29*, 1605750.
[55] Y. Zhang, H. Sun, C. K. Jeong, *ACS Appl. Mater. Interfaces* **2018**, *10*, 35539.
[56] Q. He, B. Bethers, B. Tran, Y. Yang, presented at *International Manufacturing Science and Engineering Conference*, American Society of Mechanical Engineers, New York **2022**, https://doi.org/10.1115/MSEC2022-85646.
[57] X. Zhang, F. Shi, J. Niu, Y. Jiang, Z. Wang, *J. Mater. Chem. A* **2008**, *18*, 621.
[58] M. Ran, W. Zheng, H. Wang, *Mater. Sci. Technol.* **2019**, *35*, 313.
[59] L. Feng, S. Li, Y. Li, H. Li, L. Zhang, J. Zhai, Y. Song, B. Liu, L. Jiang, D. Zhu, *Adv. Mater.* **2002**, *14*, 1857.
[60] M. Wang, Q. Liu, H. Zhang, C. Wang, L. Wang, B. Xiang, Y. Fan, C. F. Guo, S. Ruan, *ACS Appl. Mater. Interfaces* **2017**, *9*, 29248.
[61] H. Zhu, F. Yang, J. Li, Z. Guo, *Chem. Commun.* **2016**, *52*, 12415.
[62] H. Dai, C. Gao, J. Sun, C. Li, N. Li, L. Wu, Z. Dong, L. Jiang, *Adv. Mater.* **2019**, *31*, 1905449.
[63] H. Wang, Z. Zhang, J. Zheng, J. Zhao, Y. Liang, X. Li, L. Ren, *Chem. Eng. J.* **2021**, *417*, 127944.
[64] C. Zhou, Z. Chen, H. Yang, K. Hou, X. Zeng, Y. Zheng, J. Cheng, *ACS Appl. Mater. Interfaces* **2017**, *9*, 9184.
[65] V. Hejazi, K. Sobolev, M. Nosonovsky, *Sci. Rep.* **2013**, *3*, 2194.
[66] B. Balu, J. S. Kim, V. Breedveld, D. W. Hess, *J. Adhes. Sci. Technol.* **2009**, *23*, 361.
[67] H. J. Ensikat, P. Ditsche-Kuru, C. Neinhuis, W. Barthlott, *Beilstein J. Nanotechnol.* **2011**, *2*, 152.
[68] L. Feng, Y. Zhang, J. Xi, Y. Zhu, N. Wang, F. Xia, L. Jiang, *Langmuir* **2008**, *24*, 4114.
[69] P. Perez Goodwyn, Y. Maezono, N. Hosoda, K. Fujisaki, *Naturwissenschaften* **2009**, *96*, 781.
[70] M. Sun, G. S. Watson, Y. Zheng, J. A. Watson, A. Liang, *J. Exp. Biol.* **2009**, *212*, 3148.
[71] K. Liu, J. Du, J. Wu, L. Jiang, *Nanoscale* **2012**, *4*, 768.
[72] D.-M. Chun, G. Davaasuren, C.-V. Ngo, C.-S. Kim, G.-Y. Lee, S.-H. Ahn, *CIRP Ann.* **2014**, *63*, 525.
[73] M. H. Kwon, H. S. Shin, C. N. Chu, *Appl. Surf. Sci.* **2014**, *288*, 222.
[74] L. Li, J. He, J. Lei, L. Liu, X. Zhang, T. Huang, N. Li, F. Pan, *J. Taiwan Inst. Chem. Eng.* **2017**, *75*, 240.
[75] K. Maghsoudi, G. Momen, R. Jafari, M. Farzaneh, *Appl. Surf. Sci.* **2018**, *458*, 619.
[76] Y. Zeng, L. Jiang, Q. He, R. Wodnicki, Y. Yang, Y. Chen, Q. Zhou, *J. Phys. D: Appl. Phys.* **2021**, *55*, 013002.
[77] Y. Zeng, L. Jiang, Y. Sun, Y. Yang, Y. Quan, S. Wei, G. Lu, R. Li, J. Rong, Y. Chen, Q. Zhou, *Micromachines* **2020**, *11*, 713.
[78] Y. Yang, X. Li, X. Zheng, Z. Chen, Q. Zhou, Y. Chen, *Adv. Mater.* **2018**, *30*, 1704912.
[79] Q. He, H. Tang, Y. Zeng, Y. Yang, presented at *Int. Manuf. Sci. Eng. Conf.*, American Society of Mechanical Engineers, New York **2023**.
[80] J. Reza, C. Come, A. Anahaita, M. Gelareh, *Int. J. Adv. Manuf. Technol.* **2019**, *103*, 1225.
[81] Q. Yin, Q. Guo, Z. Wang, Y. Chen, H. Duan, P. Cheng, *ACS Appl. Mater. Interfaces* **2020**, *13*, 1979.
[82] Y. Li, H. Mao, P. Hu, M. Hermes, H. Lim, J. Yoon, M. Luhar, Y. Chen, W. Wu, *Adv. Mater. Technol.* **2019**, *4*, 1800638.
[83] X. Liu, H. Gu, M. Wang, X. Du, B. Gao, A. Elbaz, L. Sun, J. Liao, P. Xiao, Z. Gu, *Adv. Mater.* **2018**, *30*, 1800103.
[84] J. Bonilla-Cruz, J. A. C. Sy, T. E. Lara-Ceniceros, J. C. Gaxiola-López, V. García, B. A. Basilia, R. C. Advincula, *Soft Matter* **2021**, *17*, 7524.
[85] K. Koeltzsch, A. Dinkelacker, R. Grundmann, *Exp. Fluids* **2002**, *33*, 346.
[86] D. M. Bushnell, K. J. Moore, *Annu. Rev. Fluid Mech.* **1991**, *23*, 65.
[87] L. Wen, J. C. Weaver, G. V. Lauder, *J. Exp. Biol.* **2014**, *217*, 1656.
[88] S.-J. Lee, S.-H. Lee, *Exp. Fluids* **2001**, *30*, 153.
[89] A. Lang, P. Motta, P. Hidalgo, M. Westcott, *Bioinspir. Biomim.* **2008**, *3*, 046005.
[90] A. W. Lang, E. M. Jones, F. Afroz, *Bioinspir. Biomim.* **2017**, *12*, 026005.
[91] S. H. Ridgway, D. A. Carder, *IEEE Eng. Med. Biol. Mag* **1993**, *12*, 83.
[92] M. Hassanalian, H. Abdelmoula, S. Mohammadi, S. Bakhtiyarov, J. Goerlich, U. Javed, *J. Thermal Biol.* **2019**, *84*, 292.
[93] J. Ou, J. P. Rothstein, *Phys. Fluids* **2005**, *17*, 103606.
[94] W. Sagong, W.-P. Jeon, H. Choi, *PLoS One* **2013**, *8*, e81323.
[95] Q. Zhang, C. Sun, Y. Zhu, N. Xu, H. Liu, *Glob. Ecol. Conserv.* **2020**, *21*, e00876.
[96] A. Bottaro, *J. Fluid Mech.* **2019**, *877*, P1.
[97] D. Fan, X. Feng, G. Tian, Y. Zhang, *Langmuir* **2021**, *37*, 11804.
[98] Y. Cai, L. Lin, Z. Xue, M. Liu, S. Wang, L. Jiang, *Adv. Funct. Mater.* **2014**, *24*, 809.
[99] Y. Luo, Y. Liu, J. Anderson, X. Li, Y. Li, *Appl. Phys. A* **2015**, *120*, 369.
[100] T. Kim, R. Shin, M. Jung, J. Lee, C. Park, S. Kang, *Appl. Surf. Sci.* **2016**, *367*, 147.

[101] L. Wu, Z. Jiao, Y. Song, C. Liu, H. Wang, Y. Yan, *Sci. Rep.* **2018**, *8*, 12186.
[102] H. Chen, X. Zhang, L. Ma, D. Che, D. Zhang, T. S. Sudarshan, *Appl. Surf. Sci.* **2014**, *316*, 124.
[103] T. W. Kim, *J. Nanosci. Nanotechnol.* **2014**, *14*, 7562.
[104] Y. C. Jung, B. Bhushan, *J. Phys.: Condens. Matter* **2009**, *22*, 035104.
[105] A. G. Domel, G. Domel, J. C. Weaver, M. Saadat, K. Bertoldi, G. V. Lauder, *Bioinspir. Biomim.* **2018**, *13*, 056014.
[106] W. Dai, M. Alkahtani, P. R. Hemmer, H. Liang, *Friction* **2019**, *7*, 603.
[107] L. Wen, J. C. Weaver, P. J. Thornycroft, G. V. Lauder, *Bioinspir. Biomim.* **2015**, *10*, 066010.
[108] G. Tian, D. Fan, X. Feng, H. Zhou, *RSC Adv.* **2021**, *11*, 3399.
[109] A. S. Ramirez, M. E. I. Marcos, F. B. Haro, R. D'Amato, R. Sant, J. Porras, *Rapid Prototyping J.* **2019**, *25*, https://doi.org/10.1108/RPJ-09-2018-0251.
[110] Y. Yasuda, K. Zhang, O. Sasaki, M. Tomita, D. Rival, J. Galipon, *J. Electrochem. Soc.* **2019**, *166*, B3302.
[111] Y. Cui, D. Li, H. Bai, *Ind. Eng. Chem. Res.* **2017**, *56*, 4887.
[112] T. Tengteng, J. Dylan, L. Xiangjia, in *Advances in 3D Printing* (Eds: S. Ashutosh, Rijeka), IntechOpen, London, UK **2023**, Ch. 5
[113] T. Tang, S. Alfarhan, K. Jin, X. Li, *Adv. Funct. Mater.* **2023**, *33*, 2370029.
[114] D. Joralmon, S. Alfarhan, S. Kim, T. Tang, K. Jin, X. Li, *ACS Appl. Polym. Mater.* **2022**, *4*, 2951.
[115] S. Feng, P. Zhu, H. Zheng, H. Zhan, C. Chen, J. Li, L. Wang, X. Yao, Y. Liu, Z. Wang, *Science* **2021**, *373*, 1344.
[116] P. Zhang, L. Zhang, H. Chen, Z. Dong, D. Zhang, *Adv. Mater.* **2017**, *29*, 1702995.
[117] P. Lv, Y.-L. Zhang, D.-D. Han, H.-B. Sun, *Adv. Mater. Interfaces* **2021**, *8*, 2100043.
[118] S. Zhou, L. Jiang, Z. Dong, *Adv. Mater. Interfaces* **2021**, *8*, 2000824.
[119] M. Tenjimbayashi, K. Kawamura, S. Shiratori, *Adv. Mater. Interfaces* **2020**, *7*, 2000984.
[120] L. Wang, J. Li, B. Zhang, S. Feng, M. Zhang, D. Wu, Y. Lu, J. J. Kai, J. Liu, Z. Wang, L. Jiang, *Research* **2020**, *2020*, 6472313.
[121] C. Li, C. Yu, S. Zhou, Z. Dong, L. Jiang, *Proc. Natl. Acad. Sci. USA* **2020**, *117*, 23436.
[122] Z. Cui, L. Xiao, Y. Li, Y. Zhang, G. Li, H. Bai, X. Tang, M. Zhou, J. Fang, L. Guo, S. Liu, C. Xiao, M. Cao, *J. Mater. Chem. A* **2021**, *9*, 9719.
[123] B. Hu, Z. Duan, B. Xu, K. Zhang, Z. Tang, C. Lu, M. He, L. Jiang, H. Liu, *J. Am. Chem. Soc.* **2020**, *142*, 6111.
[124] S. Prakash, J. Yeom, *Nanofluidics and microfluidics: systems and applications*, William Andrew, Norwich, NY **2014**.
[125] X. Luanluan, L. Huizeng, L. An, Z. Zhipeng, S. Yanlin, *Prog. Chem.* **2020**, *33*, 78.
[126] T.-S. Wong, S. H. Kang, S. K. Y. Tang, E. J. Smythe, B. D. Hatton, A. Grinthal, J. Aizenberg, *Nature* **2011**, *477*, 443.
[127] A. K. Epstein, T.-S. Wong, R. A. Belisle, E. M. Boggs, J. Aizenberg, *Proc. Natl. Acad. Sci. USA* **2012**, *109*, 13182.
[128] P. Wang, D. Zhang, Z. Lu, *Colloids Surf., B* **2015**, *136*, 240.
[129] S. Jung, M. Dorrestijn, D. Raps, A. Das, C. M. Megaridis, D. Poulikakos, *Langmuir* **2011**, *27*, 3059.
[130] X. Sun, V. G. Damle, S. Liu, K. Rykaczewski, *Adv. Mater. Interfaces* **2015**, *2*, 1400479.
[131] X. Zhang, L. Sun, Y. Wang, F. Bian, Y. Wang, Y. Zhao, *Proc. Natl. Acad. Sci. USA* **2019**, *116*, 20863.
[132] K. Manabe, E. Koyama, Y. Norikane, *ACS Appl. Mater. Interfaces* **2021**, *13*, 36341.
[133] Y. Kwak, H. Y. Jun, Y. Lee, M. Kang, J. S. Oh, S. Kim, Y. H. Song, C.-H. Choi, *Ind. Eng. Chem. Res.* **2021**, https://doi.org/10.1021/acs.iecr.1c00856.
[134] P. Zhu, L. Zhu, F. Ge, G. Wang, Z. Zeng, *Surf. Coat. Technol.* **2021**, *426*, 127793.
[135] J.-X. Lu, S.-L. Wu, Z.-H. Liang, H.-C. Yang, W. Li, *ACS Appl. Mater. Interfaces* **2021**, *13*, 23134.
[136] C. Liu, Y. Li, C. Lu, Y. Liu, S. Feng, Y. Liu, *ACS Appl. Mater. Interfaces* **2020**, *12*, 25471.
[137] C. Wei, J. Yan, H. Tang, Q. Zhang, X. Zhan, F. Chen, *Prog. Chem.* **2016**, *28*, 9.
[138] Z. Lao, Y. Hu, C. Zhang, L. Yang, J. Li, J. Chu, D. Wu, *ACS Nano* **2015**, *9*, 12060.
[139] F. Zhang, H. Y. Low, *Langmuir* **2007**, *23*, 7793.
[140] Z. Ji, C. Yan, S. Ma, S. Gorb, X. Jia, B. Yu, X. Wang, F. Zhou, *Tribol. Int.* **2019**, *132*, 99.
[141] S. Zhou, C. Yu, C. Li, Z. Dong, L. Jiang, *J. Mater. Chem. A* **2019**, *7*, 18244.
[142] L. Xiao, G. Li, Y. Cai, Z. Cui, J. Fang, H. Cheng, Y. Zhang, T. Duan, H. Zang, H. Liu, S. Li, Z. Ni, Y. Hu, *Chem. Eng. J.* **2020**, *399*, 125139.
[143] Y. Si, T. Wang, C. Li, C. Yu, N. Li, C. Gao, Z. Dong, L. Jiang, *ACS Nano* **2018**, *12*, 9214.
[144] C. Li, H. Dai, C. Gao, T. Wang, Z. Dong, L. Jiang, *Proc. Natl. Acad. Sci. USA* **2019**, *116*, 12704.
[145] L. Liang, W. Wang, J. Chen, K. Jiang, Y. Sheng, X. Peng, A. Liu, H. Wu, *Materials* **2019**, *12*, 1043.
[146] L. Xiao, G. Li, Y. Cai, Z. Cui, J. Fang, H. Cheng, Y. Zhang, T. Duan, H. Zang, H. Liu, S. Li, Z. Ni, Y. Hu, *Chem. Eng. J.* **2020**, *399*, 125139.
[147] P. Comanns, G. Buchberger, A. Buchsbaum, R. Baumgartner, A. Kogler, S. Bauer, W. Baumgartner, *J. R. Soc., Interface* **2015**, *12*, 20150415.
[148] Y. Gu, L. Yu, J. Mou, D. Wu, P. Zhou, M. Xu, *e-Polymers* **2020**, *20*, 443.
[149] P. K. Szewczyk, J. Knapczyk-Korczak, D. P. Ura, S. Metwally, A. Gruszczynski, U. Stachewicz, *Mater. Lett.* **2018**, *233*, 211.
[150] A. Roth-Nebelsick, M. Ebner, T. Miranda, V. Gottschalk, D. Voigt, S. Gorb, T. Stegmaier, J. Sarsour, M. Linke, W. Konrad, *J. R. Soc., Interface* **2012**, *9*, 1965.
[151] H. G. Andrews, E. A. Eccles, W. C. E. Schofield, J. P. S. Badyal, *Langmuir* **2011**, *27*, 3798.
[152] H. Bai, J. Ju, R. Sun, Y. Chen, Y. Zheng, L. Jiang, *Adv. Mater.* **2011**, *23*, 3708.
[153] H. Bai, L. Wang, J. Ju, R. Sun, Y. Zheng, L. Jiang, *Adv. Mater.* **2014**, *26*, 5025.
[154] J. Ju, X. Yao, S. Yang, L. Wang, R. Sun, Y. He, L. Jiang, *Adv. Funct. Mater.* **2014**, *24*, 6933.
[155] L. Liu, S. Liu, M. Schelp, X. Chen, *ACS Appl. Mater. Interfaces* **2021**, *13*, 29122.
[156] L. Peng, K. Chen, D. Chen, J. Chen, J. Tang, S. Xiang, W. Chen, P. Liu, F. Zheng, J. Shi, *RSC Adv.* **2021**, *11*, 14769.
[157] J. Wang, S. Yi, Z. Yang, Y. Chen, L. Jiang, C.-P. Wong, *ACS Appl. Mater. Interfaces* **2020**, *12*, 21080.
[158] Y. Shi, O. Ilic, H. A. Atwater, J. R. Greer, *Nat. Commun.* **2021**, *12*, 2797.
[159] X. Li, Y. Yang, L. Liu, Y. Chen, M. Chu, H. Sun, W. Shan, Y. Chen, *Adv. Mater. Interfaces* **2020**, *7*, 1901752.
[160] Y. Shi, O. Ilic, H. A. Atwater, J. R. Greer, *Nat. Commun.* **2021**, *12*, 2797.
[161] J. Lv, Z. Gong, Z. He, J. Yang, Y. Chen, C. Tang, Y. Liu, M. Fan, W.-M. Lau, *J. Mater. Chem. A* **2017**, *5*, 12435.
[162] C. Yan, S. Ma, Z. Ji, Y. Guo, Z. Liu, X. Zhang, X. Wang, *Polymers* **2019**, *11*, 774.
[163] Z. Jin, H. Mei, Y. Yan, L. Pan, H. Liu, S. Xiao, L. Cheng, *J. Materiomics* **2021**, *7*, 8.
[164] X. Li, H. Shan, W. Zhang, B. Li, *Sep. Purif. Technol.* **2020**, *237*, 116324.
[165] L. D. Tijing, J. R. C. Dizon, I. Ibrahim, A. R. N. Nisay, H. K. Shon, R. C. Advincula, *Appl. Mater. Today* **2020**, *18*, 100486.
[166] A. Khalil, F. E. Ahmed, N. Hilal, *Sci. Total Environ.* **2021**, *790*, 148238.
[167] M. Zou, Y. Zhang, Z. Cai, C. Li, Z. Sun, C. Yu, Z. Dong, L. Wu, Y. Song, *Adv. Mater.* **2021**, *33*, 2102443.
[168] M. M. Badran, J. Kuntsche, A. Fahr, *Eur. J. Pharm. Sci.* **2009**, *36*, 511.

[169] M. H. Asfour, *Drug Deliv. Trans. Res.* **2021**, *11*, 1.
[170] T. Waghule, G. Singhvi, S. K. Dubey, M. M. Pandey, G. Gupta, M. Singh, K. Dua, *Biomed. Pharmacother.* **2019**, *109*, 1249.
[171] P. Dardano, A. Caliò, V. Di Palma, M. Bevilacqua, A. Di Matteo, L. De Stefano, *Materials* **2015**, *8*, 8661.
[172] K.-H. Ke, C.-K. Chung, *Small* **2020**, *16*, 2001209.
[173] A. Arora, M. R. Prausnitz, S. Mitragotri, *Int. J. Pharm.* **2008**, *364*, 227.
[174] S. Babity, M. Roohnikan, D. Brambilla, *Small* **2018**, *14*, 1803186.
[175] R. E. M. Lutton, J. Moore, E. Larrañeta, S. Ligett, A. D. Woolfson, R. F. Donnelly, *Drug Deliv. Trans. Res.* **2015**, *5*, 313.
[176] S. Henry, D. V. Mcallister, M. G. Allen, M. R. Prausnitz, *J. Pharm. Sci.* **1998**, *87*, 922.
[177] Z. F. Rad, P. D. Prewett, G. J. Davies, *Beilstein J. Nanotechnol.* **2021**, *12*, 1034.
[178] E. D. Ozyilmaz, A. Turan, T. Comoglu, *Pharm. Dev. Technol.* **2021**, *26*, 923.
[179] M. Guo, Y. Wang, B. Gao, B. He, *ACS Nano* **2021**, *15*, 15316.
[180] A. J. Shoffstall, S. Srinivasan, M. Willis, A. M. Stiller, M. Ecker, W. E. Voit, J. J. Pancrazio, J. R. Capadona, *Sci. Rep.* **2018**, *8*, 122.
[181] X. Zhang, F. Wang, Y. Yu, G. Chen, L. Shang, L. Sun, Y. Zhao, *Sci. Bull.* **2019**, *64*, 1110.
[182] X. Li, W. Shan, Y. Yang, D. Joralmon, Y. Zhu, Y. Chen, Y. Yuan, H. Xu, J. Rong, R. Dai, Q. Nian, Y. Chai, Y. Chen, *Adv. Funct. Mater.* **2021**, *31*, 2003725.
[183] J. Ling, Z. Song, J. Wang, K. Chen, J. Li, S. Xu, L. Ren, Z. Chen, D. Jin, L. Jiang, *J. Mech. Behav. Biomed. Mater.* **2017**, *68*, 173.
[184] Y. Lu, T. Ren, H. Zhang, Q. Jin, L. Shen, M. Shan, X. Zhao, Q. Chen, H. Dai, L. Yao, J. Xie, D. Ye, T. Lin, X. Hong, K. Deng, T. Shen, J. Pan, M. Jia, J. Ling, P. Li, Y. Zhang, H. Wang, L. Zhuang, C. Gao, J. Mao, Y. Zhu, *Acta Biomater.* **2022**, *153*, 386.
[185] L. M. A. Jorge, F. B. Filho, F. Lamy, L. K. A. Balassiano, L. Towersey, R. Hay, M. A. C. Frade, "Clinical manifestation, histopathology, and imaging of traumatic injuries caused by Brazilian porcupine (Sphiggurus villosus) quills," Case reports in dermatological medicine, **2016**, https://doi.org/10.1155/2016/7851986.
[186] M. A. Luzuriaga, D. R. Berry, J. C. Reagan, R. A. Smaldone, J. J. Gassensmith, *Lab Chip* **2018**, *18*, 1223.
[187] S. N. Economidou, C. P. P. Pere, A. Reid, Md. J. Uddin, J. F. C. Windmill, D. A. Lamprou, D. Douroumis, *Mater. Sci. Eng., C* **2019**, *102*, 743.
[188] X. Zhang, G. Chen, Y. Yu, L. Sun, Y. Zhao, *Research* **2020**, *2020*, 3672120.
[189] D. Han, R. S. Morde, S. Mariani, A. A. La Mattina, E. Vignali, C. Yang, G. Barillaro, H. Lee, *Adv. Funct. Mater.* **2020**, *30*, 1909197.
[190] M. Amer, R. K. Chen, *Macromol. Biosci.* **2020**, *20*, 2000089.
[191] C. Plamadeala, S. R. Gosain, F. Hischen, B. Buchroithner, S. Puthukodan, J. Jacak, A. Bocchino, D. Whelan, C. O'mahony, W. Baumgartner, J. Heitz, *Biomed. Microdev.* **2020**, *22*, 8.
[192] V. Yadav, P. K. Sharma, U. S. Murty, N. H. Mohan, R. Thomas, S. K. Dwivedy, S. Banerjee, *Int. J. Pharm.* **2021**,*605*, 120815.
[193] X. Li, W. Shan, Y. Yang, D. Joralmon, Y. Zhu, Y. Chen, Y. Yuan, H. Xu, J. Rong, R. Dai, Q. Nian, Y. Chai, Y. Chen, *Adv. Funct. Mater.* **2021**, *31*, 2003725.
[194] I. Xenikakis, K. Tsongas, E. K. Tzimtzimis, C. K. Zacharis, N. Theodoroula, E. P. Kalogianni, E. Demiri, I. S. Vizirianakis, D. Tzetzis, D. G. Fatouros, *Int. J. Pharm.* **2021**, *597*, 120303.
[195] C. Plamadeala, S. R. Gosain, F. Hischen, B. Buchroithner, S. Puthukodan, J. Jacak, A. Bocchino, D. Whelan, C. O'mahony, W. Baumgartner, J. Heitz, *Biomed. Microdevices* **2020**, *22*, 1.
[196] V. Yadav, P. K. Sharma, U. S. Murty, N. H. Mohan, R. Thomas, S. K. Dwivedy, S. Banerjee, *Int. J. Pharm.* **2021**, *605*, 120815.
[197] I. Xenikakis, K. Tsongas, E. K. Tzimtzimis, C. K. Zacharis, N. Theodoroula, E. P. Kalogianni, E. Demiri, I. S. Vizirianakis, D. Tzetzis, D. G. Fatouros, *Int. J. Pharm.* **2021**,*597*, 120303.
[198] C. Yeung, S. Chen, B. King, H. Lin, K. King, F. Akhtar, G. Diaz, B. Wang, J. Zhu, W. Sun, A. Khademhosseini, S. Emaminejad, *Biomicrofluidics* **2019**, *13*, 064125.
[199] S. N. Economidou, Md. J. Uddin, M. J. Marques, D. Douroumis, W. T. Sow, H. Li, A. Reid, J. F. C. Windmill, A. Podoleanu, *Addit. Manuf.* **2021**, *38*, 101815.
[200] I. Xenikakis, M. Tzimtzimis, K. Tsongas, D. Andreadis, E. Demiri, D. Tzetzis, D. G. Fatouros, *Eur. J. Pharm. Sci.* **2019**, *137*, 104976.
[201] Z. Chen, Y. Lin, W. Lee, L. Ren, B. Liu, L. Liang, Z. Wang, L. Jiang, *ACS Appl. Mater. Interfaces* **2018**, *10*, 29338.
[202] K. J. Krieger, N. Bertollo, M. Dangol, J. T. Sheridan, M. M. Lowery, E. D. O'Cearbhaill, *Microsyst. Nanoeng.* **2019**, *5*, 42.
[203] A. S. Cordeiro, I. A. Tekko, M. H. Jomaa, L. Vora, E. Mcalister, F. Volpe-Zanutto, M. Nethery, P. T. Baine, N. Mitchell, D. W. Mcneill, R. F. Donnelly, *Pharm. Res.* **2020**, *37*, 174.
[204] N. El-Sayed, L. Vaut, M. Schneider, *Eur. J. Pharm. Biopharm.* **2020**, *154*, 166.
[205] Z. Huang, G. Chi-Pong Tsui, Y. Deng, C.-Y. Tang, *Nanotechnol. Rev.* **2020**, *9*, 1118.
[206] S. Liu, S. Chu, G. E. Banis, L. A. Beardslee, R. Ghodssi, presented at *2020 IEEE 33rd International Conference on Micro Electro Mechanical Systems (MEMS)*, IEEE, **2020**.
[207] K. Moussi, A. Bukhamsin, T. Hidalgo, J. Kosel, *Adv. Eng. Mater.* **2020**, *22*, 1901358.
[208] Q. Geng, D. Wang, P. Chen, S.-C. Chen, *Nat. Commun.* **2019**, *10*, 2179.

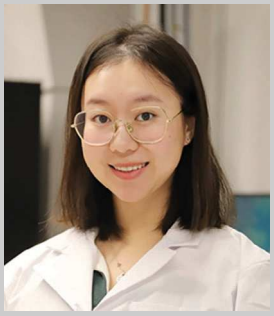

Qingqing He received the M.S. degree in Mechanical Engineering from the University of Southern California, Los Angeles, CA, USA, in 2021. She is currently pursuing the jointed Ph.D. degree with the Department of Mechanical Engineering, San Diego State University & University of California, San Diego, CA, USA. Her research interests mainly focus on the bio-inspired 3D-printed functional materials, and development of advanced 3D printing technologies.

Tengteng Tang is a Ph.D. candidate in the Department of Aerospace and Mechanical Engineering at Arizona State University. He received his B.S. degree in Mechanical Engineering at Hefei University of Technology (2020). His research interests mainly focus on biomimetic additive manufacturing (3D printing), employing vat photopolymerization, functional composite materials, and multi-physics fields to fabricate multi-scale and multi-functional structures for the application in self-sensing device, superhydrophobic surface, and optical steganography. He is the 2023-2024 Mistletoe Research Fellow.

Yushun Zeng, ACS / IEEE Graduate Student member, received the B.Eng. degree in Bioengineering from Nanjing Tech University, Nanjing, China, in 2019, and the M.S. degree in Biomedical Engineering from the University of Southern California, Los Angeles, CA, USA, in 2021. He is currently pursuing the Ph.D. degree with the Department of Biomedical Engineering, University of Southern California, Los Angeles, CA, USA. His research interests mainly focus on the fabrication of high-frequency ultrasound transducer/array, ultrasound stimulation, ultrasound-induced energy harvesting, 3D-printed advanced ultrasonic device, and development of high-frequency acoustic tweezer for cell manipulation.

Cindy (Xiangjia) Li is an assistant professor in the department of mechanical and aerospace engineering at the School for Engineering of Matter, Transport, and Energy at Arizona State University. She successfully earned her Ph.D. in Industrial and Systems Engineering from the University of Southern California in 2019. Her research focuses on photopolymerization-based additive manufacturing, utilizing bioinspired design methodologies, and the development of programmable functional materials. These areas of study hold great promise for potential applications in interfacial technology, biomedical engineering, soft actuators, optics, and flexible electronics. Dr.Li's recent work has garnered significant recognition, including the prestigious Best Paper awards at ASME MSEC2022 and MSEC2023. Additionally, she has been honored with the 2023 SME Delcie R. Durham Outstanding Young Manufacturing Engineer Award.

Yang Yang is an Assistant Professor in the Department of Mechanical Engineering at San Diego State University. His research focuses on the machine, materials, and structures development for bioinspired 3D printing. He received his B.S. in Physics from Wuhan University in 2009. He completed the joint Ph.D. at Wuhan University and University of California, Los Angeles (UCLA) in Physics and Bioengineering in 2015. Prior to joining SDSU, Dr. Yang is a Postdoc at The University of Southern California (USC) in the Department of Industrial and Systems Engineering and Center for Advanced Manufacturing. He has received the '2022 SME Sandra L. Bouckley Outstanding Young Manufacturing Engineer Award' and has authored over 50 peer-reviewed publications. His work has been supported by NSF and SDSU seed grants.